

Design Strategies for Dendrite-Free Potassium Metal Batteries

Yanchang Chen, Jie Wen, Xianhui Yi, Ling Fan, Jiang Zhou, and Bingan Lu*

Potassium metal batteries (KMBs) have emerged as a promising next-generation energy storage technology, offering superior energy density and cost-effectiveness compared to conventional graphite-based potassium (K)-ion batteries. However, the practical implementation of KMBs faces significant challenges, primarily due to the high reactivity of K metal anodes and uncontrollable growth of K dendrites, which lead to poor cycling stability and serious safety concerns. In recent years, there has been substantial progress in both the fundamental understanding and experimental advancements in KMB research. Herein, recent developments in

K metal anodes are highlighted and potential regulatory mechanisms and strategies to improve the cycling performance of KMBs are summarized. These strategies include the 3D confinement strategies, artificial solid-electrolyte interface design, modification of current collectors, separator design, and electrolyte engineering. Finally, the opportunities and potential future directions for the application of K metal anodes are discussed. This review aims to provide a comprehensive resource for researchers working toward the development of high-performance KMBs for next-generation energy storage systems.

1. Introduction

Energy plays a pivotal role in the advancement of modern society, and research into electrochemistry energy storage devices has remained a relentless focus. Alkaline (Li, Na, and K)-ion batteries have emerged as a critical energy storage technology and have been extensively studied in recent years.^[1] Given concerns over the supply and geopolitical challenges associated with lithium resources, rechargeable battery technologies based on K⁺ and Na⁺ have attracted growing attention.^[2–4] This is due to their placement in the same main group as Li and their similar properties, particularly their identical outermost electron configurations. Compared to lithium resources, both sodium and potassium resources are far more abundant in the Earth's crust, with natural abundances of 0.0017, 2.3, and 2.1 wt% for Li, Na, and K, respectively. The Li and K exhibit similar standard redox potentials relative to the standard hydrogen electrode (SHE), with values of –3.04 V versus SHE for Li⁺/Li and –2.94 V versus SHE for K⁺/K, both of which are lower than that of Na⁺/Na (–2.79 V vs. SHE). Additionally, in propylene carbonate (PC)-based electrolytes, the redox potential of the K⁺/K (–2.88 V) is the lowest compared to those of Li⁺/Li (–2.79 V) and Na⁺/Na (–2.56 V), enabling higher operation voltage and energy densities in potassium-ion batteries (KIBs). Furthermore, the Lewis acidity of K⁺ is weaker

than that of Li⁺ and Na⁺, resulting in a smaller Stokes radius in the PC solvent (K⁺: 3.6 Å < Na⁺: 4.6 Å < Li⁺: 4.8 Å). Consequently, K⁺ exhibits the highest ionic mobility, conductivity, and transport number, endowing KIBs with the potential for high-power performance.^[5,6]

Research on anode materials is of paramount importance in rechargeable battery systems. During the charging and discharging processes, anode materials serve as carriers for ions and electrons, playing a critical role in storing and releasing energy. Currently, investigations into anode materials for K⁺ storage are advancing rapidly, with significant progress being made in understanding storage mechanisms, structural design, and performance optimization. Ideal anode materials for KIBs should exhibit characteristics such as high specific capacity, low operating voltage, excellent cycling stability, and low cost. Since the first experimental demonstration in 2015 that K⁺ can intercalate into graphite at low potentials, numerous anode materials have been extensively designed and explored to enhancing the energy density of KIBs (e.g., carbon, organics, oxides, alloys, etc.) (Figure 1a).^[7–26] Based on the K⁺ storage mechanism, the anodes of KIBs can be divided into several main types: 1) K metal; 2) alloys (e.g., Ge, Sb, and SnSb); 3) intercalation materials (e.g., graphite and TiO₂); and 4) conversion materials (e.g., WS₂, MoS₂, and SnS₂). It is well established that a low working voltage in the anode can significantly improve the overall voltage and energy density of the full battery when combined with a cathode. Among anode materials, K metal stands out due to its exceptionally low working voltage and impressive reversible capacity (theoretical: 687 mAh g^{–1}), setting it apart from other anode options.^[27]

Although potassium metal batteries (KMBs) have broad application prospects, they still face multiple technical challenges. The chemistries and main issues of several KMBs are summarized in Figure 1b. In K metal-based battery systems (e.g., KMBs, K-S, and K-O₂ batteries), the K dendrite growth represents a ubiquitous failure mechanism.^[28–30] Particularly noteworthy is that the

Y. Chen, J. Wen, X. Yi, L. Fan, B. Lu

School of Physics and Electronics
Hunan University
Changsha 410082, China
E-mail: luba2012@hnu.edu.cn

J. Zhou
School of Materials Science and Engineering and Key Laboratory of Nonferrous Metal Materials Science and Engineering
Ministry of Education
Central South University
Changsha 410083, China

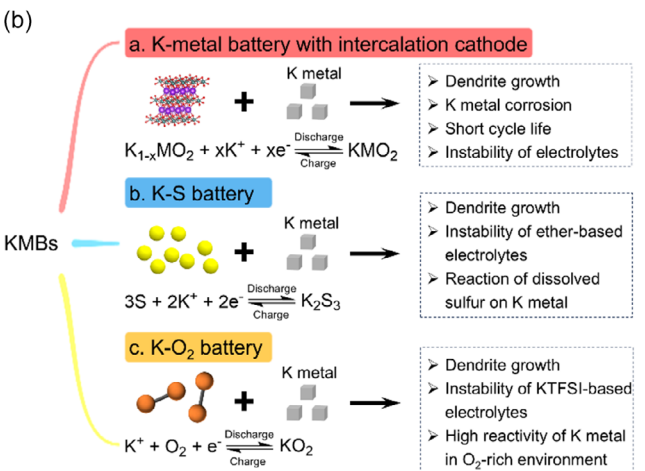
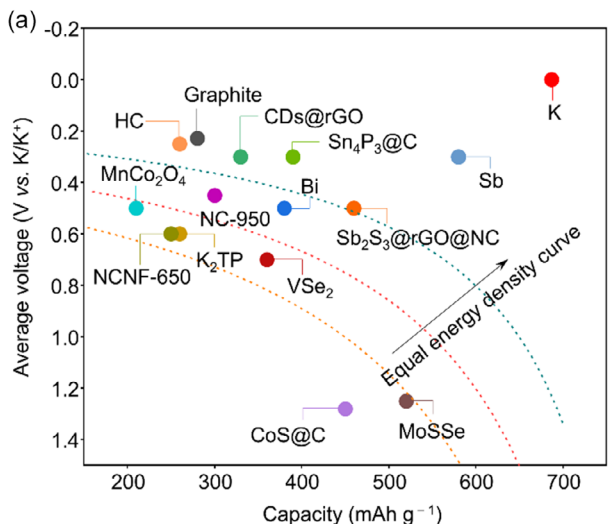


Figure 1. a) A summary of the capacity-average voltage for various anode materials. b) Application and key challenges of KMBs.

polysulfide shuttle effect in K-S batteries^[29] leads to persistent corrosion of K metal by polysulfide anions, while the superoxide radical anions generated through oxygen reduction reactions in K-O₂ batteries^[30] induce more severe parasitic reactions. Compared to conventional intercalation-type cathodes, these conversion-type batteries (K-S/K-O₂) present dual challenges for metal anode protection, they require not only dendrite suppression but also the construction of effective interfaces to resist active species attack. Despite these complex interfacial issues, achieving stable cycling of K metal anodes remains central to realizing the potential of such high-energy-density batteries, as their theoretical energy density fundamentally relies on high specific capacity and low redox potential of K metal. Rational regulation of K metal anode electrochemical behavior presents both scientific excitement and significant challenges. While dendrite growth is a common issue with all alkali metal anodes, K dendrite formation is particularly severe due to the high reactivity of K metal.^[31] Furthermore, potassium's lattice parameter is 34% larger than that of lithium (0.533 nm for K vs. 0.351 nm for Li), a result of

the inherent physical differences between the two elements.^[5] This larger lattice parameter leads to more pronounced electrode expansion and contraction during K metal plating and stripping. Such significant volume changes increase the likelihood of solid-electrolyte interface (SEI) rupture, which in turn heightens the risk of K dendrites penetrating the SEI and the battery separator.

Currently, research on KMBs is a rapidly advancing field, driven by their potential to address the growing demand for high-energy-density and cost-effective energy storage solutions. As such, it is crucial to provide a timely and comprehensive summary of the latest research progress to guide the future development of KMBs. This review delves various strategies and working principles aimed at achieving superior electrochemical performance in KMBs, which are categorized into five key areas: the 3D confinement strategies, artificial SEI (ASEI), modification of current collectors, separator design, and electrolyte engineering. It also provides a detailed overview of representative and cutting-edge research achievements in these areas. By synthesizing the latest advancements and identifying key research gaps, this



Yanchang Chen received his B.E. from Xiangtan University in 2021. Currently, he is pursuing his M.S. at Hunan University. His research interests focus on potassium (K) metal batteries.



Jie Wen received his bachelor's degree in college of chemistry and chemical engineering from Hunan University in 2019. His research interests mainly focus on the potassium ion batteries, such as, exploration of functionalized electrolytes, preparation of electrode materials, and construction of potassium-ion full batteries.



Bingan Lu received his Ph.D. from Lanzhou University in 2012. Currently, he is a professor at School of Physics and Electronics, Hunan University. His research interests mainly focus on designing functionalized electrode materials and electrolytes of metal (Li, Na, K, Al, Zn) ion batteries.

review aims to offer valuable insights and a scientific outlook for further advancements in K-metal-based battery systems, ultimately contributing to the realization of next-generation energy storage technologies.

2. Modification Strategies for K Metal Anodes

In recent years, direct modification of K metal anodes has emerged as a highly effective and straightforward solution. This approach primarily encompasses three key strategies: 3D porous frameworks, ASEL, and modifications to current collectors. These methods are designed to enhance K^+ plated behavior,

optimize electron/ion conduction, and improve interfacial properties. The modification of K metal anodes shows significant research value and promising application potential, particularly in addressing the critical challenge of K dendrite growth in KMBs. To provide a comprehensive overview, we begin by examining the current benchmarks in modified K metal anodes, specifically in $K||K$ symmetrical cells. Figure 2a summarizes relevant reported data, including modification methods, cycling time, areal current density, and areal capacity.^[32–82] A quantitative analysis detailing the electrolyte compositions and their corresponding performance parameters is provided in Table 1. From 2018 to 2024, researchers have extensively explored practical applications of K metal anodes through diverse approaches,

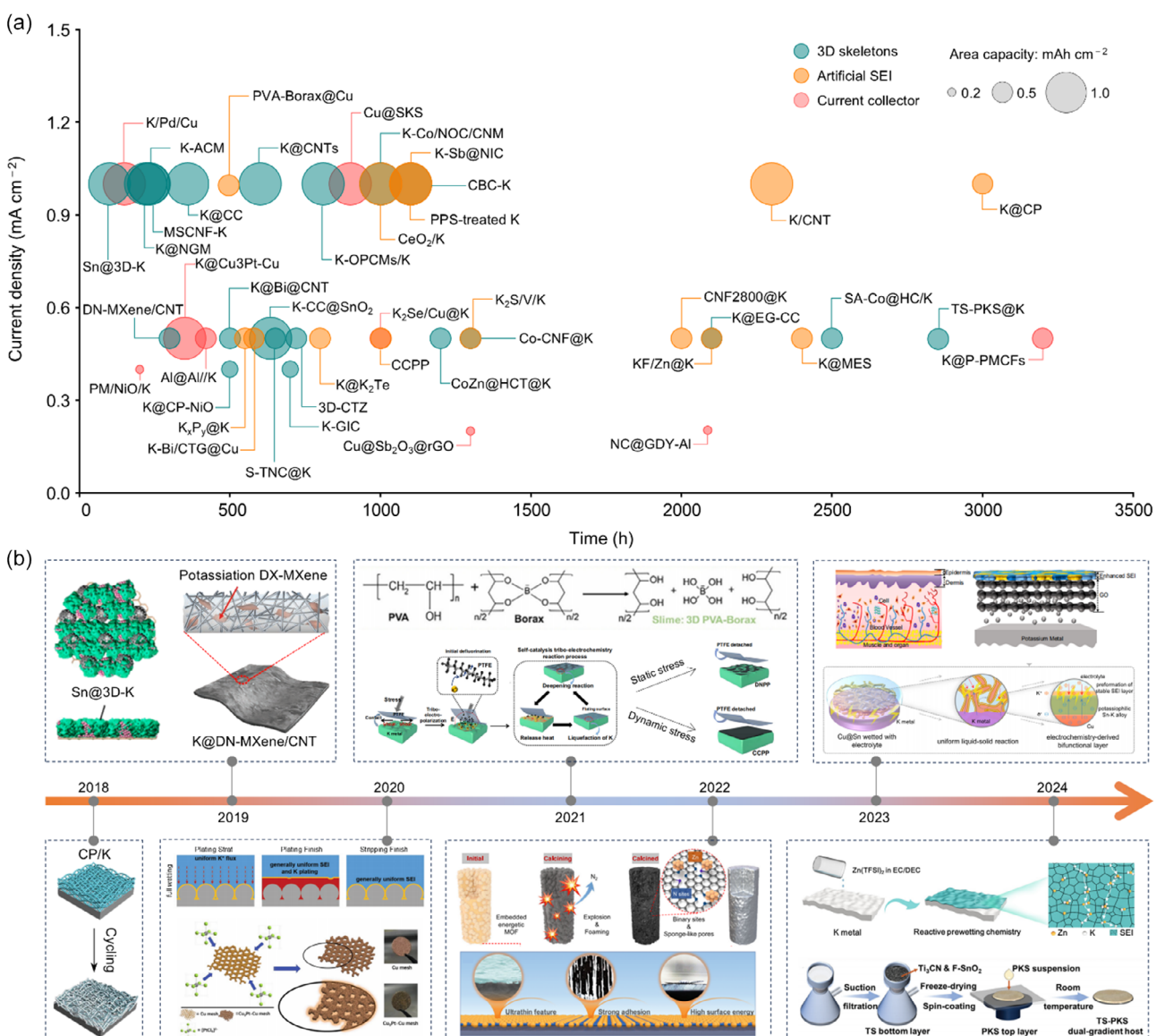


Figure 2. a) Recent advancements in electrochemical performance and modification strategies for K metal anodes. b) A timeline illustrating the evolution of K metal anode modification techniques. Materials in (b) are Reproduced with permission.^[55] Copyright 2018, Elsevier B.V. Reproduced with permission.^[59] Copyright 2019, American Chemical Society. Reproduced with permission.^[49] Copyright 2019, Wiley-VCH Verlag GmbH & Co. KGaA, Weinheim. Reproduced with permission.^[39] Copyright 2020, Wiley-VCH GmbH. Reproduced with permission.^[60] Copyright 2020, Elsevier Ltd. Reproduced with permission.^[34] Copyright 2021, Wiley-VCH GmbH. Reproduced with permission.^[33] Copyright 2021, The Author(s). Reproduced with permission.^[61] Copyright 2022, The Author(s). Reproduced with permission.^[75] Copyright 2022, Wiley-VCH GmbH. Reproduced with permission.^[63] Copyright 2023, The Author(s). Reproduced with permission.^[64] Copyright 2023, American Chemical Society. Reproduced with permission.^[42] Copyright 2023, The Authors. Reproduced with permission.^[65] Copyright 2024, Wiley-VCH GmbH.

Table 1. A literature survey of different K metal anode protection methods.

Method	Material	Areal Current Density [mA cm ⁻²]	Areal Capacity [mAh cm ⁻²]	Cycling Time [h]	Electrolyte
Current Collector	PM-NiO-K ^[74]	0.4	0.2	200	1 M KPF ₆ /EC-DMC
	Al@Al ^[56]	0.5	0.5	420	4 M KFSI/DME
	K@Cu ₃ Pt-Cu ^[76]	0.5	3	350	1 M KPF ₆ /EC-DMC + FEC
	K ₂ Se-Cu@K ^[50]	0.5	0.5	1000	1 M KFSI/EC-DEC
	Pd@Cu foam ^[75]	1	1	150	3 M KFSI/DME
	Cu@SKS ^[42]	1	1	900	4 M KFSI/DME
	Cu@Sb ₂ O ₃ @rGO ^[71]	0.2	0.2	1300	3 M KFSI/DME
	K@P-PMCF ₅ ^[40]	0.5	0.5	3200	1 M KFSI/EC-DEC
	Al@G ^[58]	0.5	0.5	1000	4 M KFSI/DME
	MCNF ^[37]	1	1	1100	1 M KFSI/EC-DEC
3D Skeletons	Cu-OSe NWs ^[65]	1	1	950	4 M KFSI/DME
	Cu ₆ Sn ₅ @Cu ^[51]	1	1	600	4 M KFSI/DME
	ACM ^[45]	1	1	230	0.8 M KPF ₆ /EC-DEC
	K@DN-MXene-CNT ^[44]	0.5	0.5	300	0.8 M KPF ₆ /EC-DEC
	Sn@3D-K ^[43]	1	1	100	5 M KFSI/DME
	a-Ti ₃ C ₂ ^[77]	5	10	700	0.8 M KFSI/EC-DEC
	CBC ^[36]	1	1	1100	5 M KFSI/DME
	CC@SnO ₂ ^[72]	0.2	1	635	1 M KFSI/EC-DEC
	Co-CNF ^[32]	0.5	0.5	1300	1 M KFSI/DME
	K-GIC ^[67]	0.4	0.4	700	0.8 M KPF ₆ /EC-DEC
ASEI	CoZn@HCT ^[33]	0.5	0.5	1200	1 M KFSI/EC-DEC
	K@CC ^[41]	1	1	360	0.8 M KFSI/EC-DEC
	K@CNTs ^[35]	1	1	222	2.5 M KFSI/EC-DEC
	K@NGM ^[62]	1	1	220	0.5 M KFSI/DME
	MSCNF-K ^[78]	1	1	233	1 M KFSI/EC-DEC
	SA-Co@HC-K ^[49]	0.5	0.5	2500	3 M KFSI/EC-DEC
	3D-CTZ ^[73]	0.5	0.5	720	1 M KFSI/DME
	K-Co-NOC-CNM ^[53]	1	1	1000	1 M KFSI/EC-DEC
	K-OPCMs ^[52]	1	1	810	3 M KFSI/DME
	O-CC ^[64]	0.5	0.5	5500	5 M KFSI/DME
PVA-Borax@Cu ^[59]	K@CP-NiO ^[61]	0.4	0.4	500	1 M KFSI/DMC
	K@EG-CC ^[82]	0.5	0.5	2100	1.5 M KFSI/EC-DEC
	S-TNC@K ^[70]	0.5	0.5	650	1 M KFSI/DME
	TS-PKS@K ^[48]	0.5	0.5	2900	1 M KFSI/DME
	CP@K ^[66]	1	0.5	3000	1 M KPF ₆ /EC-DMC
	CNT ^[47]	1	1	2300	0.5 M KPF ₆ /EC-DEC
	K _x P _y @K ^[46]	0.5	0.5	550	1 M KTFSI/EC-DEC
	K ₂ Te@K ^[57]	0.5	0.5	800	1 M KFSI/EC-DEC
	PTFE ^[80]	0.5	0.5	1000	3 M KFSI/EC-DEC
	CNF2800@K ^[60]	0.5	0.5	2000	1 M KFSI/EC-DEC
Bi-CTG@Cu ^[63]	K ₂ S-V-K ^[55]	0.5	0.5	1300	1 M KFSI/EC-DEC
	PPS ^[38]	1	1	1100	1 M KFSI/DME
	CeO ₂ @K ^[34]	1	1	1000	3 M KFSI/EC-DEC
	F-GO ^[79]	0.5	0.5	2400	3 M KFSI/DME
	KF-Zn@K ^[68]	0.5	0.5	580	1 M KFSI/DME
	K-Sb@NIC ^[54]	1	1	2100	1 M KFSI/EC-DEC
				1100	1 M KFSI/EC-DEC

including the development of 3D porous frameworks, the integration of current collectors with scaffold materials, and the fabrication of ASEI using organic or inorganic components (Figure 2b).^[42–44,48,56,58,59,66,68,76,78–80] To provide a clear and systematic understanding of the strengths and limitations of each modification method, we present them in a detailed and structured manner.

2.1. 3D Confinement Strategies for K Metal Anodes

For 3D frameworks, the following characteristics are required: 1) cost-effectiveness and ease of fabrication, ensuring scalability and practicality for practical applications; 2) low mass density and electrochemical stability, which contribute to increasing the energy density of KMBs; 3) high surface area, which reduces local current density in accordance with Sand's law, thereby improving the structural stability of the electrode; and 4) strong compatibility with K metal, preserving the mechanical integrity of the composite electrode and preventing degradation.

Carbon-based materials, such as carbon nanotubes (CNTs), graphene, carbon fiber (CFs), carbon cloth (CC), carbon paper, and porous carbon (PC), are among the most widely used 3D framework materials.^[35,47,66,72] Early approaches included the introduction of K metal into aligned CNT membranes (ACM) by melt infusion strategy.^[45] However, pure carbon-based materials often face significant challenges, including rapid capacity decay, high nucleation sites, and high-energy barriers during the diffusion process. Building on various carbon materials, modifications have been introduced to create potassophilic sites using both metallic (e.g., M/MOx, where M = Co, Fe, Ni, Zn, Sn, Bi, etc.)^[43,49,63,68,74] and nonmetallic elements (such as N, O, and F).^[41,64,79] These modifications exhibit distinct structural characteristics, each offering specific performance advantages. It was quickly discovered that heteroatom doping, due to the strong adsorption capabilities at heteroatom sites, could significantly enhance potassium storage capacity.^[83] Nonmetallic atom modifications typically increase the number of surface defects, expand the specific surface area, and increase the specific capacity.^[64] Additionally, the doped nonmetallic atoms can form stable covalent bonds with carbon atoms, further improving the material's performance.^[41] Mai et al. demonstrated that highly potassophilic amine groups could rapidly transform carbon scaffolds from nonwetting to wetting with respect to potassium.^[41] Regarding the strategy of metallic atom doping, it can enhance electronic conductivity, thereby enabling uniform K^+ flux during the plating/stripping process and effectively suppressing the irregular growth of K dendrites.^[74] Cheng et al. reported that using Bi@CNT as a host for K metal resulted in K||K symmetrical cells with exceptional cycling stability, exhibited cycling performance for over 500 h at 0.5 mA cm^{-2} with a capacity of 0.5 mAh cm^{-2} , and exhibited significantly lower overpotential of 53 mV.^[69]

Compared to single-element doping, multielement codoping offers the potential to address more complex challenges effectively. Li et al. introduced the synthesis and application of nitrogen (N) and zinc (Zn) codoped PC nanofibers as effective hosts for

K metal.^[78] The preparation process of this material and the synthesis route for the K composite anode are illustrated in Figure 3a. Remarkably, homogeneous K metal thermal infusion was achieved in less than 1 s, highlighting the exceptional potassophilicity of the host material (Figure 3b). The calculated binding energies of K atoms with different hosts (Figure 3c–f) and the electric field distributions (Figure 3g–j) demonstrate that the Zn-triazole metal-organic framework (MOF) MET ($[\text{Zn}(\text{C}_2\text{N}_3\text{H}_2)_2]$)-derived carbon nanofibers denoted as MSCNFs is conducive to the uniform deposition of K metal, thus eliminating the growth of irregular K dendrites (Figure 3k). Tests of K||K symmetrical cells confirm the effectiveness of this strategy. As shown in Figure 3l, at a cutoff capacity of 1 mAh cm^{-2} and a current density of 1 mA cm^{-2} , the MSCNF-K||MSCNF-K symmetrical cell achieved a low average overpotential of $\approx 100 \text{ mV}$ and stable cycling for over 800 h. In comparison, the Cu-K||Cu-K symmetrical cell short circuited after $\approx 32 \text{ h}$. In the rate performance test, when the current density was increased from 0.5 to 5 mA cm^{-2} , the MSCNF-K||MSCNF-K symmetrical cell maintained stable plating and stripping. In contrast, the Cu-K||Cu-K cell short-circuited immediately when the current density was restored to 1 mA cm^{-2} (Figure 3m).

2.2. ASEI for K Metal Anodes

A smooth electrode interface is crucial for achieving uniform, dendrite-free deposition of K metal.^[84] However, inherent defects on the surface of K metal electrodes result in significant roughness. Moreover, the fragile and defective SEI is insufficient to fully inhibit further chemical or electrochemical reactions with the electrolyte. An ideal SEI should exhibit uniformity, stability, density, and robustness.^[85] It must facilitate rapid ion transport while effectively blocking electron transfer from the anode to the electrolyte, thereby protecting the K metal from extensive corrosion. Coating a protective layer (ASEI) on the electrode surface is a straightforward, versatile, and highly effective strategy to mitigate undesired interface reactions and stabilize the plating and stripping processes of K metal.^[86] To date, various materials have been explored as potential candidates for ASEI, including carbon-based materials,^[47,66] K₂S, Sn, P, Te, and CeO₂.^[34,38,46,55,57]

Dense and stable SEI can be formed through the spontaneous potassiation of carbon-based materials. Simultaneously, the resulting K-carbon compounds, which exhibit potassophilic properties, facilitate the uniform distribution of K^+ flux. Ding et al. used fluorine-doped graphene oxide (F-GO) to fabricate a double-layer protective layer on the K metal electrode surface (K@MES) through a rolling process (Figure 4a).^[79] This structure enhances the flatness of the K metal electrode, ensures uniform electric field distribution, and effectively inhibits the growth of K dendrites (Figure 4b). By COMSOL simulations of electric field effects on K^+ deposition revealed that the MES-coated surface exhibits more uniform electric field distribution, which promotes uniform K deposition on the electrode surface (Figure 4c). To address internal stress issues during K deposition, Song et al. developed a PC barrier layer with uniformly dispersed CoWO₄ nanoparticles (CoWO₄ NPs/PC, Figure 4d) via a cold-rolling technique.^[87] Density functional theory (DFT) calculations revealed

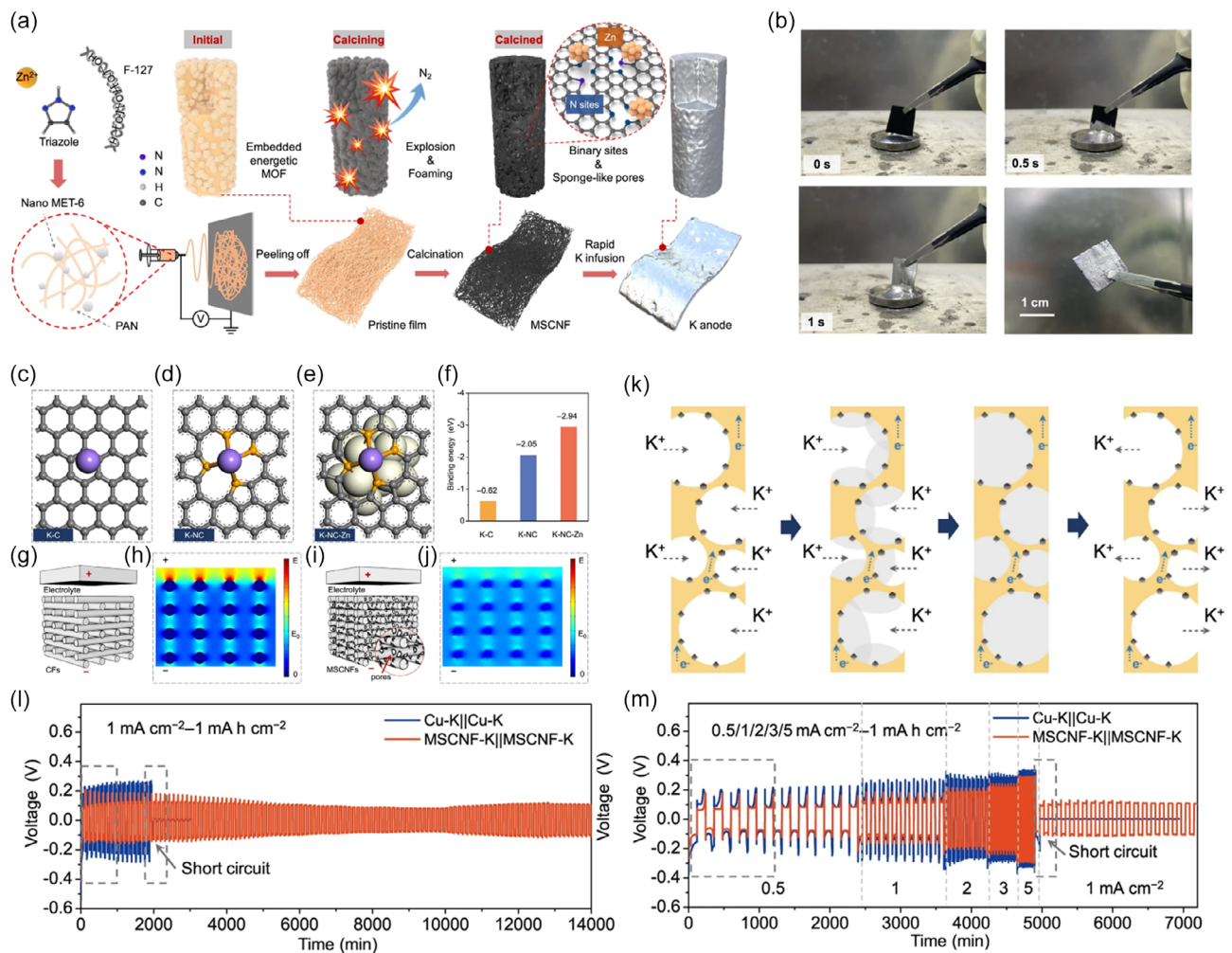


Figure 3. 3D confinement strategy for dendrite-free KMBs. a) Schematic of the preparation method for MSCNFs and the corresponding composite K metal anode. b) Optical images of K metal thermal infusion experiments conducted at 150 °C. Reproduced with permission.^[61] Copyright 2022, The Author(s). c–f) Calculated binding energies of K atoms with different hosts using DFT. Simulation model and electric field distribution of g,h) CFs and i,j) MSCNFs. k) Schematic illustration of K plating and stripping on MSCNFs. l,m) Electrochemical performance of Cu-K||Cu-K and MSCNF-K||MSCNF-K symmetric cells.

that this composite architecture not only provides abundant active sites for K deposition but significantly enhances interfacial binding characteristics with K⁺ (Figure 4e), demonstrating its dual capability in synergistically accelerating K⁺ diffusion kinetics and inducing selective deposition. Furthermore, Young's modulus measurements confirmed that the incorporation of CoWO₄ NPs improved the flexibility of the PC, providing a fundamental basis for effectively mitigating stress accumulation during cycling (Figure 4f). While rich defect carbon-based ASEIs enhance K⁺ affinity, they concurrently amplify interfacial catalytic activity toward solvent decomposition, destabilizing the chemical composition of in situ-formed SEI layers. To address this dilemma, Deng et al. developed amorphous carbon with controllable defects (SC-1600) as an ASEI to balance potassiophilicity and catalytic activity.^[88] DFT calculations demonstrate that ethylene carbonate (EC) and diethyl carbonate (DEC) solvent molecules exhibit significantly lower adsorption energies at defect sites compared to KFSI (Figure 4g). This preferential adsorption increases the proportion of organic components in the SEI,

severely compromising interfacial robustness (Figure 4h). Furthermore, such defect sites significantly reduce the K⁺ adsorption energy barrier, thereby lowering the K nucleation overpotential. Through rational modulation of ASEI defect sites, K dendrite formation can be effectively suppressed (Figure 4i).

2.3. Modification of Current Collectors

The current collector can carry the active substance and collect and output the current generated by the active substance. Modifying the interface between the current collector and K metal can regulate the K⁺ flux, effectively suppressing the irregular growth of K dendrites and mitigating side reactions between K metal and the electrolyte.^[75] An ideal current collector should be lightweight, possess high electrical conductivity and mechanical strength, exhibit excellent compatibility with the active material, and demonstrate superior stability. Common design strategies for current collectors include surface etching, coating, and the use of specialized foils. Xie et al. developed a bifunctional

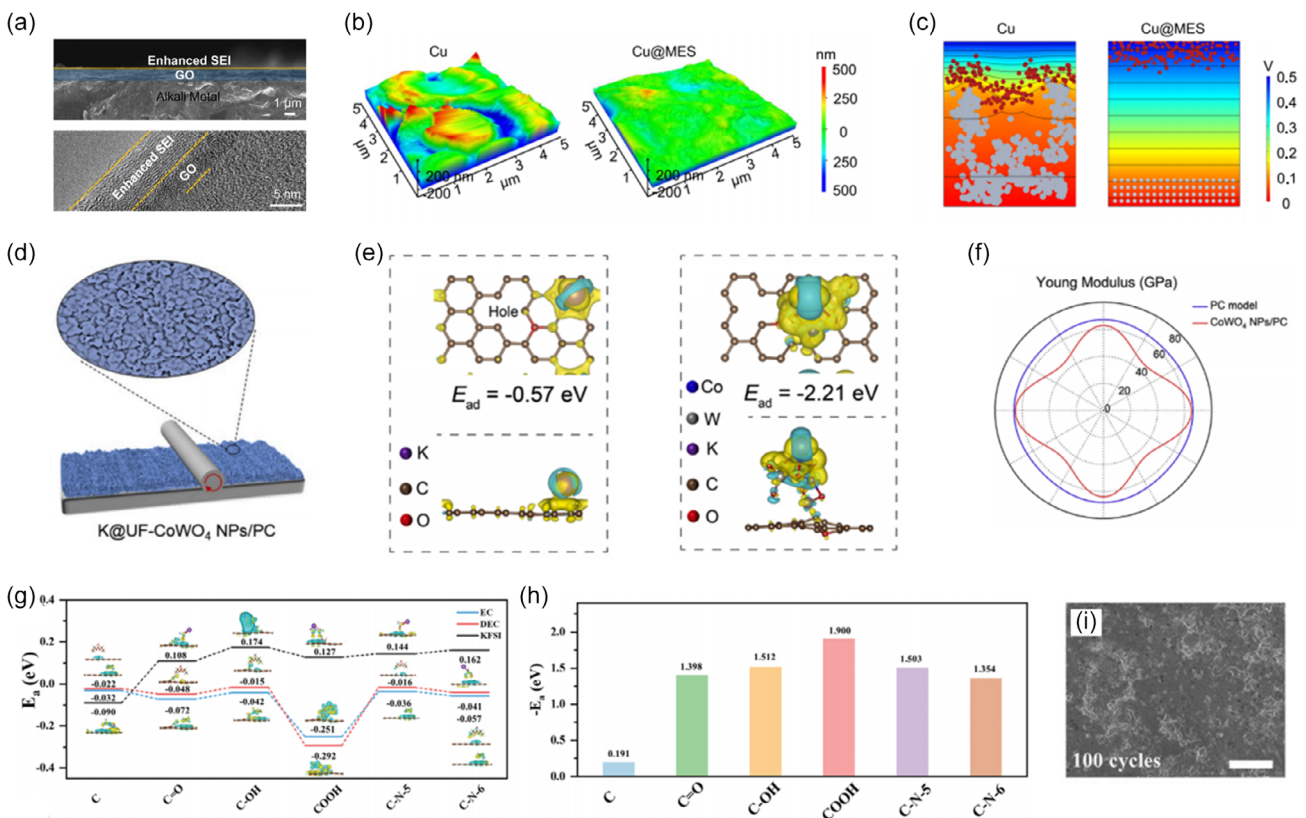


Figure 4. Preparation and characterization of ASEI. a) Scanning electron microscope (SEM) image of K@MES electrode and transmission electron microscopy image of the enhanced SEI layer. b) Atomic force microscopy (AFM) images of Cu foil surface and F-GO on the Cu foil surface. c) During the initial K plating stage, the electrode surface electric field and corresponding ion distribution. Reproduced with permission.^[63] Copyright 2023, The Author(s). d) Schematic illustration of ASEI fabrication integrating K@UF-CoWO₄ NPs/PC composites demonstrates. e) Charge density difference and adsorption energy values for K⁺ on PC and CoWO₄ NPs/PC. f) Distributions of Young's modulus. Reproduced with permission.^[86] Copyright 2024, Elsevier B.V. g) The binding energy of EC, DEC, and KFSI on different carbon configuration sites. h) The adsorption energies of K⁺ on different carbon configuration sites. i) SEM image of SC-1600@K after 100 cycles. Reproduced with permission.^[87] Copyright 2024, Wiley-VCH GmbH.

layer rich in O/F on the current collector through prepassivation, consisting of a Sn-K alloy and a preformed SEI (referred to as Cu@SKS) (Figure 5a,b).^[42] SEM images and elemental distribution maps (Figure 5c,d) reveal that K elements are uniformly distributed around the mixed Sn and K on Cu@SKS. In contrast, on pure Cu foam, K metal deposits unevenly, forming K dendrite clusters that penetrate the separator. These results demonstrate that the prepassivation process of Cu@SKS effectively promotes the homogeneous deposition of K metal, while the thinner host structure further suppresses volume expansion during K metal cycling. Charge density difference calculations (Figure 5e) and binding energy analyses (Figure 5f) of K⁺ adsorption sites on Cu (111) and KSn (112) surfaces confirm the stability of the Sn-K alloy, with SnK identified as the most stable configuration, acting as effective electron adsorption centers within the alloy. Additionally, simulations of K metal deposition morphology on different substrates highlight the prepassivation layer's ability to effectively inhibit the irregular growth of K dendrites (Figure 5g).

In their study on specialized foils, Liu et al. pioneered the use of aluminum (Al) powder-coated Al foil ("Al@Al") as a current collector for K metal anodes, marking the first successful implementation of an Al-based material for this purpose.^[44] While Al foil offers distinct advantages over Cu-based current collectors in

terms of cost-effectiveness and reduced weight, conventional commercial Al current collectors present significant challenges. These include electrochemical potassiphobic behavior and high nucleation resistance, which contribute to uneven electrochemical deposition of K metal. This results in poor reversibility during plating/stripping processes, as reflected in low Coulombic efficiency (CE). Therefore, it is crucial to regulate the nucleation and growth behavior of K metal on Al current collectors through scalable and precise surface modification strategies. Zhao et al. developed a novel approach by decorating commercial Al foil with an ultrathin graphene-modified layer (Al@G) using roll-to-roll plasma-enhanced chemical vapor deposition, which demonstrated significantly enhanced potassiphilicity (Figure 6a,b).^[58] The Al@G substrate demonstrated significantly enhanced K wettability (Figure 6c–e), as confirmed by SEM characterization, which revealed a uniform K metal deposition on the Al@G surface without K dendrites formation (Figure 6f–h). These observations indicate that the Al@G modification effectively promotes the ordered plating/stripping of K metal. Although anode-free KMBs offer enhanced energy density, they impose more stringent requirements on the K plating/stripping efficiency at the current collectors. To address this challenge, researchers assembled anode-free KMBs using FeS₂ as the cathode material and Al@G

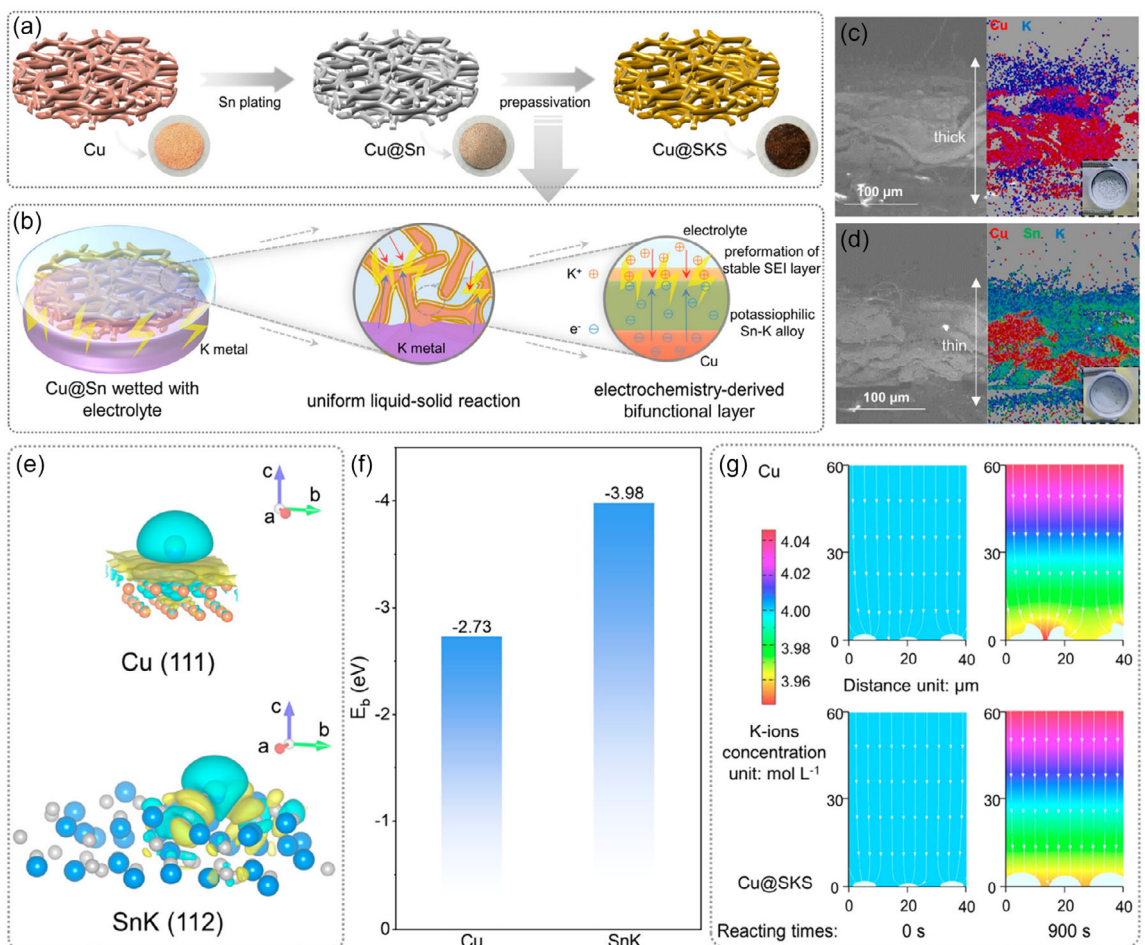


Figure 5. Modification of current collectors. a) Schematic illustration of the preparation process and the b) detailed prepassivation procedure for Cu@SKS. c,d) Cross-sectional SEM images for Cu and Cu@SKS, along with their corresponding element distribution maps. e) Differential charge density at K⁺ adsorption sites on Cu (111) and KSn (112) surfaces. f) Calculated binding energies of K atoms with Cu and Sn-K alloy using DFT. g) Surface morphology simulations of K metal deposition under uneven and even exchange current densities for Cu and Cu@SKS at 0 and 900 s, respectively. Reproduced with permission.^[64] Copyright 2023, American Chemical Society.

as the anode substrate. As shown in Figure 6*i*, the K-FeS₂||Al@G battery system exhibits a marginally decreasing trend in reversible capacity when compared to both K-FeS₂||Al and K-FeS₂||Al@C battery systems. Additionally, Li et al. proposed a carbonaceous host featuring narrowly distributed mesopores (MCNF) as a current collector for anode-free KMBs (Figure 6*j*).^[37] The anode-free KMBs, utilizing MCNF as the anode and Prussian blue (PB) as the cathode, exhibit exceptional stability in the potassium bis(Fluoromethanesulfonyl)imide (KFSI)/1,2-dimethoxyethane (DME)-1,1,2,2-tetrafluoroethyl-2,2,3,3-tetrafluoropropylether (TTE) electrolyte. The MCNF||PB cell demonstrated stable cycling for 100 cycles at 20 mA g⁻¹ with a capacity retention rate of 86%. In contrast, the Cu||PB cell, used as a control, failed within 20 cycles (Figure 6*k,l*).

3. Separator Design

During the charge/discharge process of an alkali metal battery, the anode is in direct contact with the separator, and ions shuttle between the anode and cathode through the separator's pores.

Since the electrolyte is confined within these pores, the ion flux becomes uneven and concentrated near the pore regions. Any protrusion on an inhomogeneous separator can serve as an initiation site for dendrite growth, while uneven electrolyte wetting further aggravates the nonuniform ion flux, accelerating the formation of dendrites. An effective separator can facilitate the formation of a stable SEI layer and prevent its breakdown during charge/discharge cycles, thereby significantly enhancing the battery's cycle life. Additionally, the separator's mechanical strength and flexibility enable it to withstand the volume changes that occur during battery operation, ensuring the structural integrity of the battery. In K metal anode batteries, the separator not only influences the performance and safety of the battery but also plays a pivotal role in determining its cycle life and overall efficiency. Therefore, the selection and design of suitable separator materials represent a critical step in the development of high-performance KMBs.

For separators modification, Liu et al. developed a novel multifunctional separator by double-coating microscale AlF₃ onto a polypropylene separator (AlF₃@PP) (Figure 7a).^[89] Timelapse images of the wetting behavior (Figure 7b,c) demonstrate that

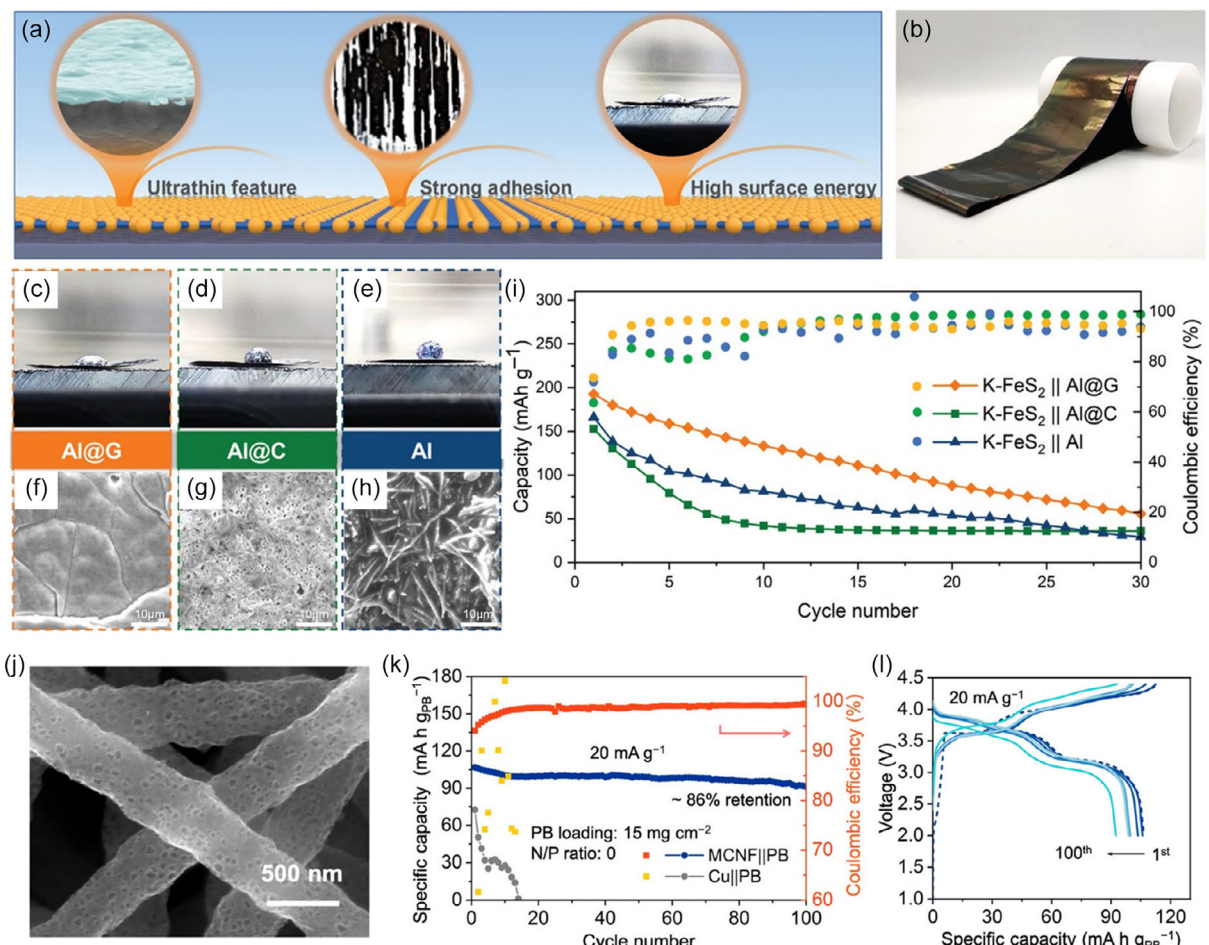


Figure 6. Anode-free KMBs. a) Schematic representation of main features of Al@G. b) Photograph of the large-scale synthesized Al@G current collectors. The wetting test of molten K metal on the c) Al@G, d) Al@C, and e) Al current collectors. f–h) Top-view SEM images after plating 2.0 mAh cm⁻² of K metal. i) Cycling performance of anode-free full cells at 100 mA g⁻¹. Reproduced with permission.^[75] Copyright 2022, Wiley-VCH GmbH. j) SEM images of the MCNF structure. k) Cycling performance of an anode-free full cells and l) corresponding voltage profiles. Reproduced with permission.^[66] Copyright 2023, American Chemical Society.

the AlF₃@PP separator exhibits significantly enhanced wettability compared to the standard PP separator. This improvement is attributed to the partial reaction of AlF₃ with K metal, which forms an SEI composed of KF, AlF₃, and Al₂O₃ phases. When using the AlF₃@PP separator, K||K symmetric cells achieved stable cycling for over 2000 h at 0.5 mA cm⁻² and 0.5 mAh cm⁻², maintaining a low overpotential of 42 mV (Figure 7d). For the structural design of separators, Wang et al. developed a hierarchical porous cellulose (HPC) separator using natural supramolecular structure engineering.^[90] The HPC separator exhibits significant advantages over glass fiber separators, including superior mechanical properties, reduced thickness, higher porosity, and an optimized structure. As shown in Figure 7e–i, the HPC separator displayed excellent recovery after undergoing curling, folding, twisting, kneading, and pinching. In terms of thermal stability, the HPC separator showed no shrinkage after being heated at 100 °C for 8 h and at 125 °C for 30 min, with only minimal shrinkage observed after exposure to 150, 175, and 200 °C for 30 min (Figure 7j). Furthermore, thermogravimetric (TG) analysis revealed that the HPC separator experienced only a 5% weight loss before reaching 200 °C. The HPC separator demonstrates

exceptional flexibility and thermal stability, ensuring it is robust enough to prevent contact between the positive and negative electrodes, even under high-temperature conditions that could otherwise cause shrinkage and lead to battery short circuits. Overall, given the limited research on separators in KMBs, the development of novel separators with enhanced compatibility with K metal anodes represents a promising and impactful research direction. Currently, glass fiber is the most commonly used separator material in K-based batteries. However, its mass and volume directly impact the gravimetric and volumetric energy densities of the battery. Therefore, this issue must be carefully considered during the design and modification of separators.

4. Electrolyte Engineering

4.1. Organic Electrolytes

In battery systems, the electrolyte should exhibit high ionic conductivity, excellent interfacial formation capability, high chemical

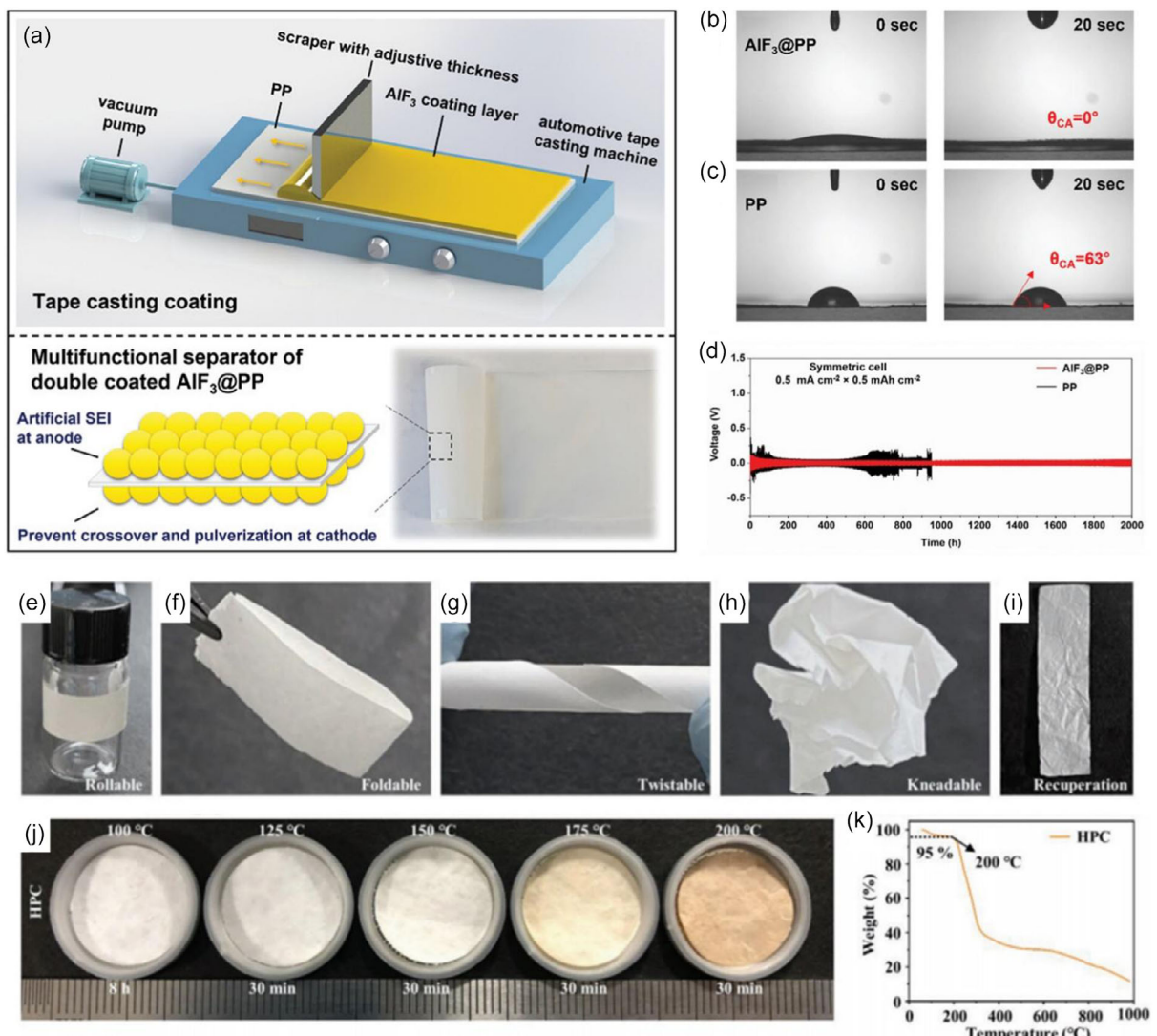


Figure 7. Fabrication of multifunctional separator. a) Schematic illustration of AlF_3 -modified multifunctional PP separator. Contact angle measurements showing the electrolyte wetting behavior on b) $\text{AlF}_3@\text{PP}$ and c) PP. d) Electrochemical performance of K||K symmetric cells. Structural design of the separator. Reproduced with permission.^[58] Copyright 2021, Wiley-VCH GmbH. e–i) Optical images the flexibility of the HPC separators. j) Thermal shrinkage of the HPC separator at various temperatures. k) TG analysis of the HPC separator. Reproduced with permission.^[89] Copyright 2022, Wiley-VCH GmbH.

stability, wide electrochemical window, and the ability to inhibit dendrite growth.^[91] For KMBs, the most significant challenge lies in the uncontrolled growth of K dendrites.^[92] To date, the reported liquid electrolytes for KMBs can be categorized into low-concentration electrolytes (LCEs), high-concentration electrolytes (HCEs), localized high-concentration electrolytes (LHCEs), and weak-solvation electrolytes (WSEs).^[93] The solvation structures and properties of these electrolyte types differ significantly, with the primary goal being the construction of anion-rich solvation sheaths to stabilize the K metal–electrolyte interface (Figure 8a). Additionally, electrolyte design must consider factors such as voltage window, ionic conductivity, viscosity, cost, and compatibility with K metal (Figure 8b). The CE of K||Cu asymmetric cells is a direct indicator for evaluating the compatibility between electrolytes and K metal anodes. Table 2 systematically summarizes recent advancements in electrolyte systems. Salts and solvents constitute the primary components of the electrolyte.

In the following section, we will delve deeper into their effects on electrolyte performance.

4.1.1. Salts

The range of available potassium salts reported to date remains relatively limited, including KFSI, potassium bis(trifluoromethanesulfonyl)imide (KTFSI), potassium hexafluorophosphate (KPF_6), potassium tetrafluoroborate (KBF_4), and potassium perchlorate (KClO_4). Notably, the solubility of KBF_4 and KClO_4 is particularly restricted (<0.5 M in PC solvent) (Figure 9a). Due to their low solubilities in typical aprotic solvents, KClO_4 and KBF_4 are rarely employed as electrolyte salts. Furthermore, the ionic conductivity of the electrolyte is significantly influenced by the type and concentration of the potassium salts (Figure 9b).^[94] Due to its excellent electrochemical stability and ability to passivate Al foil,

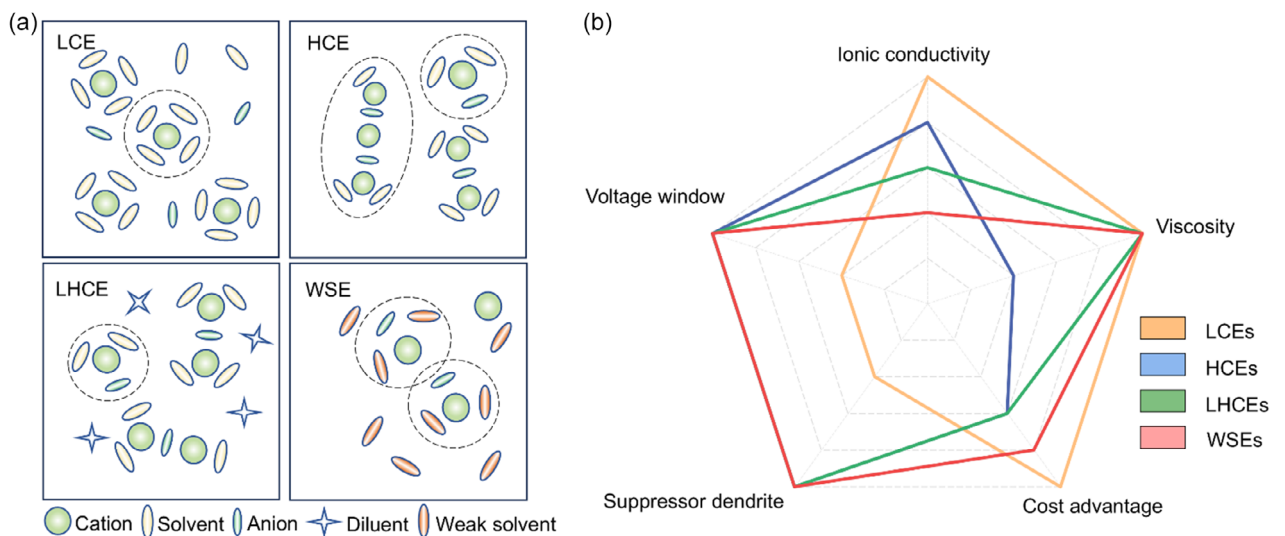


Figure 8. a) Schematic illustration of the electrolyte solvation structure from the LCE, HCE, LHCE, and WSE. b) Comparative analysis of the properties of different electrolyte types.

Table 2. Comparison of K||Cu asymmetric cell performance.

Types	Electrolyte	Area Current Density [mA cm ⁻²]	Area Capacity [mAh cm ⁻²]	CE [%]	Cycle Number [n]
LCEs	0.8 M KPF ₆ /EC-DEC-PC ^[129]	0.5	0.5	72	100
	0.8 M KHFDF/EC-DMC ^[96]	0.25	0.5	94.3	200
	0.5 M KFSI/EC-DEC ^[130]	0.5	0.5	97.5	100
	1 M KFSI/DME ^[99]	0.05	0.15	99	100
HCEs	4.34 M KFSI/DME ^[131]	1	1	97.9	700
	4 M KFSI/DEGDME ^[101]	0.25	0.25	98.3	400
	3 M KFSI/DME ^[133]	0.1	0.1	98.6	100
	3.29 M KFSI/TMP ^[110]	0.2	–	99.8	50
LHCEs	0.6 M KFSI/TPP-TFP-OHE ^[132]	0.25	0.5	99.45	400
	1 M KFSI/TMP-DX ^[93]	0.25	0.5	97.74	60
	1 M KFSI/DME-MME-OOE ^[103]	0.1	0.2	98	260
	2.8 M KFSI/DME-TTE ^[134]	0.05	0.05	98	800
	1.6 M KFSI/DME-TTE ^[37]	0.05	0.15	99.3	740
	2 M KFSI/DEM-DME ^[135]	0.5	0.5	99.4	400
	1.5 M KFSI/DPGDME-DBE ^[136]	0.1	0.1	99.9	400
	1.5 M KFSI/DGM-DBE ^[106]	0.25	0.5	98.4	200
WSEs	1 M KFSI/TMP-TEP-TTE-OTE-HFME ^[104]	0.5	1.0	99.39	400
	1 M KFSI/TFP ^[112]	0.1	0.5	96.5	500
	0.91 M KFSI/DEEC ^[114]	0.25	0.5	98.27	400
	1 M KFSI/DMM ^[115]	0.2	0.4	98.66	400
	2 M KFSI/DEE ^[137]	0.2	0.4	98.9	550
	1 M KFSI/FEMC-FEC ^[117]	0.5	0.5	90	90

KPF₆-based electrolytes are widely used in KIBs. However, the instability of the SEI formed by KPF₆-based electrolytes limits their further application in KMBs. Research has shown that, compared to KPF₆-based electrolytes, KFSI electrolytes can form a more stable SEI layer on the anode surface, significantly enhancing anode performance. Nevertheless, typical KFSI-based electrolytes tend to corrosion Al foil at high potentials, and thus,

they are primarily employed in research on KMBs operating at potentials below 4 V. Furthermore, KTFSI is costly, tends to corrosion Al foil at high potentials, and exhibits poor compatibility with K metal compared to KFSI.^[95] As a result, its application in KMBs is significantly limited. The limited diversity of anion species has persistently hindered the further development of KMBs.

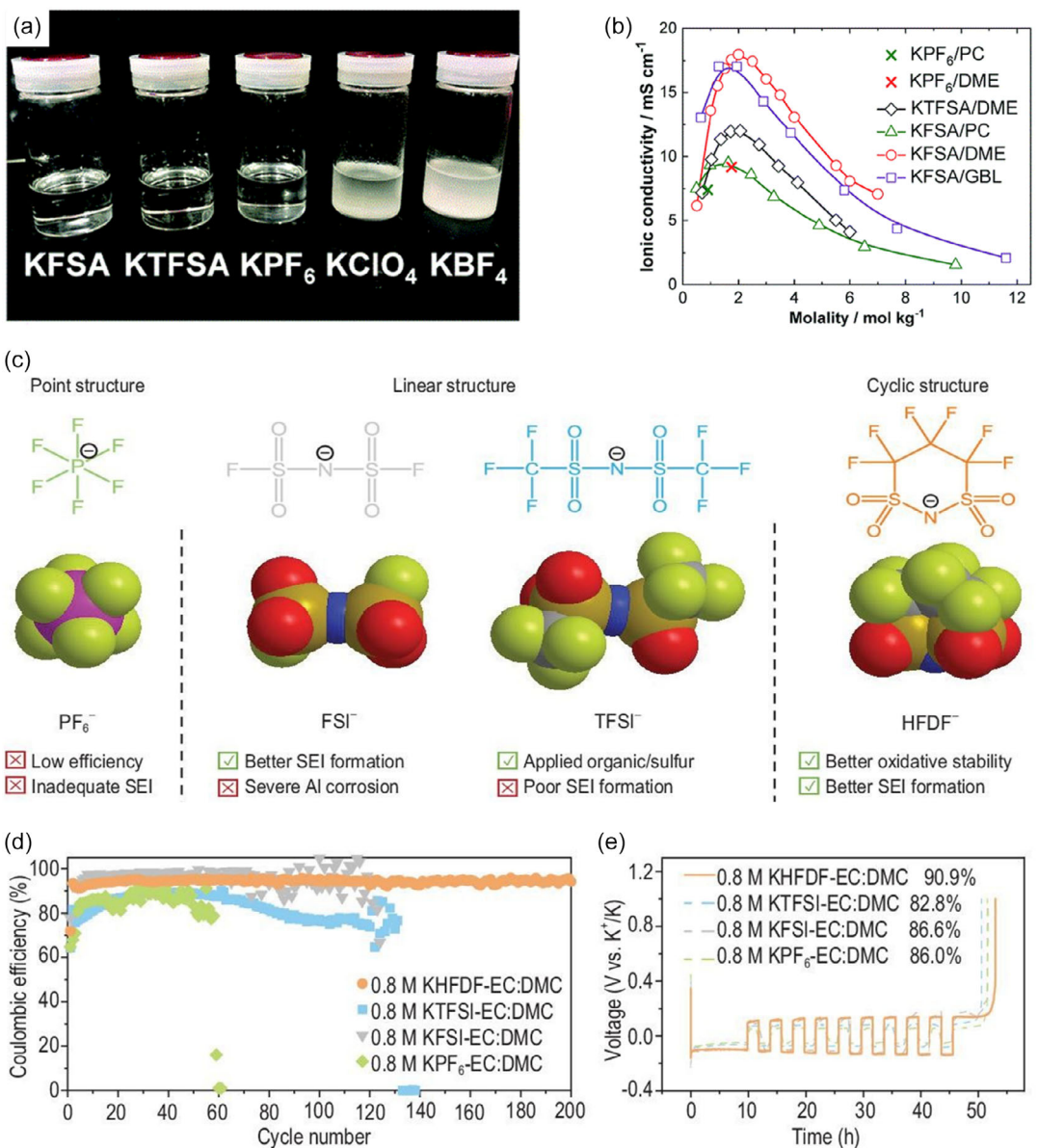


Figure 9. Design strategies for potassium Salts. a) Photograph of KFSA, KTFSA, KPF₆, KBF₄, and KClO₄ as potassium salts for 0.5 M PC-based electrolytes. b) Relationship between molar concentration and ionic conductivity under room temperature. Reproduced with permission.^[117] Copyright 2018, Royal Society of Chemistry. c) Design scheme and molecular structure of different anions. d) Cycling performance and e) Aurbach efficiency of K metal in K||Cu asymmetric cells with different electrolytes. Reproduced with permission.^[129] Copyright 2022, The Author(s).

Hu et al. developed a new electrolyte system based on the cyclic hexafluoropropane-1,3-disulfonimide anion (HFDF⁻) and successfully implemented it in KMBs (Figure 9c).^[96] The research team conducted a comprehensive comparative analysis conventional anion-based electrolytes, including linear KFSI, KTFSI, and point KPF₆-based electrolyte systems. The evaluation focused on several critical performance metrics, including electrochemical stability, high-voltage properties, and compatibility with K metal. Among the four investigated electrolyte systems, the 0.8 M KHFDF in EC-dimethyl carbonate (DMC) electrolyte demonstrated superior performance in symmetric and asymmetric cells, exhibiting enhanced CE, extended cycle life, and stability (Figure 9d,e). This remarkable performance can be attributed to the relatively low energy level of the lowest unoccupied molecular orbital

(LUMO) of the HFDF⁻ anion, which facilitates the formation of a uniform and stable SEI during K plating/stripping processes, effectively preventing the formation of dead K. Through comprehensive characterization using sputtering X-ray photoelectron spectroscopy (XPS) and time-of-flight secondary ion mass spectrometry, the composition of formed SEI in different electrolyte systems was systematically investigated. The analysis revealed that the SEI layer derived from the KHFDF-based electrolyte is predominantly composed of KF with a minor fraction of C-containing organic species, which exhibit a homogeneous distribution throughout the entire depth of the SEI layer. In contrast, conventional electrolyte systems typically form a stratified SEI structure, characterized by an organic-rich outer layer and an inorganic-dominated inner layer. Furthermore, owing to the

unique cyclic structural of the HFDF^- anion, the HFDF-based electrolyte demonstrates exceptional oxidative stability at high voltages up to 4.7 V, along with excellent compatibility with Al foil current collectors.

4.1.2. Solvents

The electrochemical stability of an electrolyte system plays a pivotal role in determining both the cycle life and safety performance of batteries, as it is intrinsically linked to the fundamental characteristics of the electrolyte. In the context of solvent selection, the electrochemical stability window is primarily governed by the energy levels of the highest occupied molecular orbital (HOMO) and the LUMO, which dictate the oxidation and reduction potentials, respectively (Figure 10a).^[97] A comparative analysis of SEI formation mechanisms in ether-based and carbonate-based electrolytes was conducted by DFT calculations, focusing on the energy levels of the HOMO and LUMO.^[98]

As shown in Figure 10b, the FSI^- exhibits lower LUMO energy levels and reduction potentials compared to the DME solvent in ether-based electrolytes, resulting in the formation of a more compact and inorganic-rich SEI layer predominantly derived from anion decomposition. In contrast, in carbonate-based electrolyte systems, the closely aligned LUMO energy levels of the FSI^- anion and solvent molecules trigger extensive decomposition and parasitic side reactions. This electrochemical behavior ultimately leads to the formation of an organic-dominated SEI layer with compromised structural integrity and electrochemical performance. Extensive theoretical simulations and experimental investigations have consistently demonstrated that ether-based electrolytes exhibit superior compatibility with K metal anodes compared to their carbonate-based electrolytes. This remarkable compatibility advantage primarily stems from the lower reduction potential of ether solvents, which facilitates the formation of a more stable, anion-derived SEI layer.

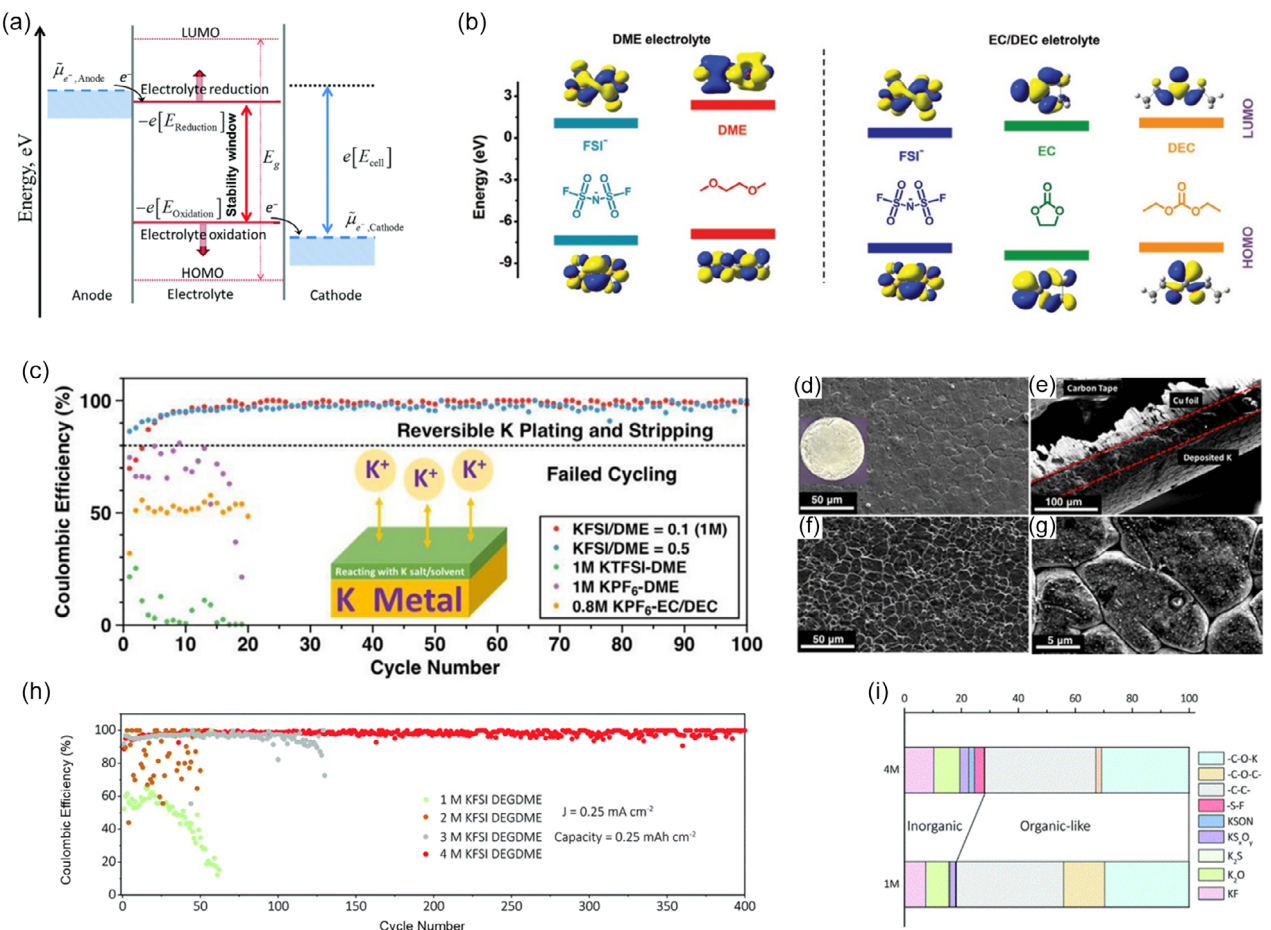


Figure 10. Strategic design approaches for electrolyte solvents. a) Illustration of electrolyte oxidation and reduction stability, accompanied by the corresponding energy levels of the HOMO and LUMO. Reproduced with permission.^[95] Copyright 2013, The Royal Society of Chemistry. b) Comparative analysis of molecular energy levels for HOMO and LUMO across various components in carbonate-based and ether-based electrolyte systems. Reproduced with permission.^[97] Copyright 2018, Wiley-VCH Verlag GmbH & Co. KGaA, Weinheim. c) Electrochemical cycling performance of K||Cu asymmetric cells employing different electrolytes, tested at a current density of 0.05 mA cm^{-2} . d–g) SEM images depicting both top-view and cross-sectional morphologies of electrochemically deposited K metal (3 mAh cm^{-2}) at different current densities in the 1 M KFSI/DME electrolyte. Reproduced with permission.^[130] Copyright 2017, American Chemical Society. h) Cycling performance evaluation of K||Cu asymmetric cells with DEGDME-based electrolytes at different concentrations. i) The calculated percent composition of surface products on the K metal anode. Reproduced with permission.^[131] Copyright 2021, The Royal Society of Chemistry.

Xiao et al. conducted a systematic investigation into the reversibility of K metal plating and stripping in various electrolyte systems.^[99] The research findings revealed that among the tested electrolyte formulations, the ether-based electrolyte comprising DME solvent and KFSI salt demonstrated distinctive advantages, emerging as the sole electrolyte system capable of achieving long-term stable and reversible K metal plating/stripping. Even in the 1 M KFSI/DME electrolyte, the K||Cu asymmetric cell demonstrated remarkable cycling stability, stable cycle over 100 cycles with an average CE of 99% (Figure 10c). The SEM characterization reveals the formation of a remarkably flat and uniform K metal deposition layer on the substrate when using the 1 M KFSI/DME electrolyte (Figure 10d–g). Although low-concentration ether-based electrolytes demonstrate certain advantages in stabilizing K metal anodes, their inherent oxidative decomposition voltage (<4 V) severely restricts their application in KMBs full cell systems. This limitation manifests primarily in the following aspects: 1) incompatibility with high-voltage cathode materials, such as layered transition metal oxides; 2) constrained operating voltage window, thereby limiting energy density; and 3) susceptibility to electrolyte decomposition at high potentials, leading to battery performance degradation. Consequently, the development of new electrolyte systems must simultaneously maintain excellent stability with K metal anodes while addressing the insufficient oxidative stability issue.

Increasing the salt concentration in electrolytes effectively reduces the number of free solvent molecules, thereby significantly suppressing the decomposition tendency of solvents under high voltage and substantially increasing the oxidative decomposition voltage of the electrolyte.^[100] For instance, Xiao et al. demonstrated that increasing the concentration of KFSI salt from 1 to 5 M could remarkably elevate the oxidative voltage from 3.5 V versus K⁺/K to 5 V versus K⁺/K.^[99] Furthermore, Xu et al. systematically investigated the impact of HCEs on anode stability, revealing that the incompatibility issue (low CE and poor cycling stability) between the low-concentration KFSI/diethylene glycol dimethyl ether (DEGDME) system and K metal could be significantly mitigated by increasing the KFSI salt concentration, leading to improved CE and cycling stability in K||Cu asymmetric cells (Figure 10h).^[101] Through Raman and XPS characterization analyses of the solvation structure and SEI composition, the results indicated that HCEs tend to form contact ion pairs and aggregate ion pairs (AGGs). This unique solvation structure facilitates the preferential decomposition of anions, resulting in the formation of a more stable and inorganic-rich SEI (Figure 10i). Although HCEs demonstrate unique advantages in stabilizing the anode and enhancing oxidative voltage, their high salt concentration nature also introduces a series of challenges. As the electrolyte concentration increases, its viscosity rises significantly, and wettability decreases markedly, which may lead to reduced ion migration speed, consequently affecting the overall conductivity of the electrolyte and the comprehensive performance of the battery.

A promising strategy to reduce the intrinsic viscosity of HCEs involves the introduction of noncoordinating diluents to form LHCEs.^[102] Yi et al. developed an innovative LHCE system comprising 1 M KFSI in a mixed solvent of DME, 3-methoxyperfluoro(2-

methylpentane) (MME), and 1,1,2,2,5,5,6,6-octafluoro-3-oxahexane (OOE).^[103] Through DFT calculations, they analyzed the binding energies between K⁺ and solvent molecules (Figure 11a). MME and OOE solvents exhibit weaker binding energies with K⁺ compared to DME solvent, a characteristic that is consistent with the fundamental properties of non-coordinating diluents. Furthermore, molecular dynamics (MD) simulations elucidated the distribution of K⁺ solvation species (Figure 11b). In comparison to the 1 M KFSI/DME electrolyte, the 1 M KFSI/DME-MME-OOE electrolyte demonstrated significantly enhanced coordination capability between K⁺ and FSI⁻. SEM images reveal the K metal plating and stripping behaviors in different electrolytes at a current density of 0.1 mA cm⁻², demonstrating that the LHCE promotes smoother K plating and effectively inhibits the growth of K dendrites (Figure 11c,d). Benefiting from the anion-derived inorganic-rich SEI facilitated by the 1 M KFSI/DME-MME-OOE electrolyte system, the K||K symmetric cells exhibited remarkable cycling stability, maintaining cycling performance for over 12 months. Additionally, Yuan et al. innovatively proposed an entropy-repaired strategy to construct a moderately weakly solvated high-entropy LHCE.^[104] This system employs trimethyl phosphate (TMP) and triethyl phosphate (TEP) as solvents, TTE, 1H,1H,5H-perfluoropentyl-1,1,2-tetrafluoroethylether (OTE), and fluoromethyl-1,1,1,3,3-hexafluoroisopropyl ether (HFME) with high compatibility with K metal as diluents. Leveraging the solvation structure reconstruction mechanism enabled by high-entropy solvents, this electrolyte significantly enhances interfacial compatibility with K metal anodes. The K||Cu asymmetric cell demonstrated an average CE of 99.39% over 400 cycles, while the K||K symmetric cell achieved ultrastable cycling for over 416 days under conditions of 0.5 mA cm⁻² current density and 1.0 mAh cm⁻² areal capacity.

Although the incorporation of noncoordinating, highly fluorinated ether solvents is an effective strategy for enhancing cycling stability of batteries, the prohibitively high cost of these fluorinated compounds remains a significant concern. To address this limitation, Wen et al. proposed an innovative approach utilizing nonfluorinated antisolvents.^[93] By incorporating a cost-effective, nonfluorinated antisolvent (1,4-dioxane) into the phosphate-based electrolyte system, the solvation structure of K⁺ was effectively optimized, resulting in a significant enhancement in the electrochemical performance of the batteries. Furthermore, due to the weak Lewis acidity of K⁺, their relatively weak interactions with solvent molecules significantly reduce salt dissociation upon the addition of diluents. Consequently, compared to lithium-ion batteries electrolytes systems, the amount of diluent required in KIBs electrolytes systems is considerably more limited.

Due to the salt deposition issue in LHCEs, conventional solutions alleviate this problem by reducing salt concentration. However, such adjustments often lead to a decline in the proportion of AGGs, resulting in limited electrochemical stability windows. Therefore, future research on LHCEs urgently requires the development of novel nonfluorinated diluents that can maintain salt solubility and AGG ratios while effectively enhancing the high-voltage stability of electrolytes.^[105] Notably, Shen et al. innovatively utilized the cosolvent effect between 1,2-dibutoxyethane (DBE) and diethylene glycol dimethyl ether (DGM), significantly

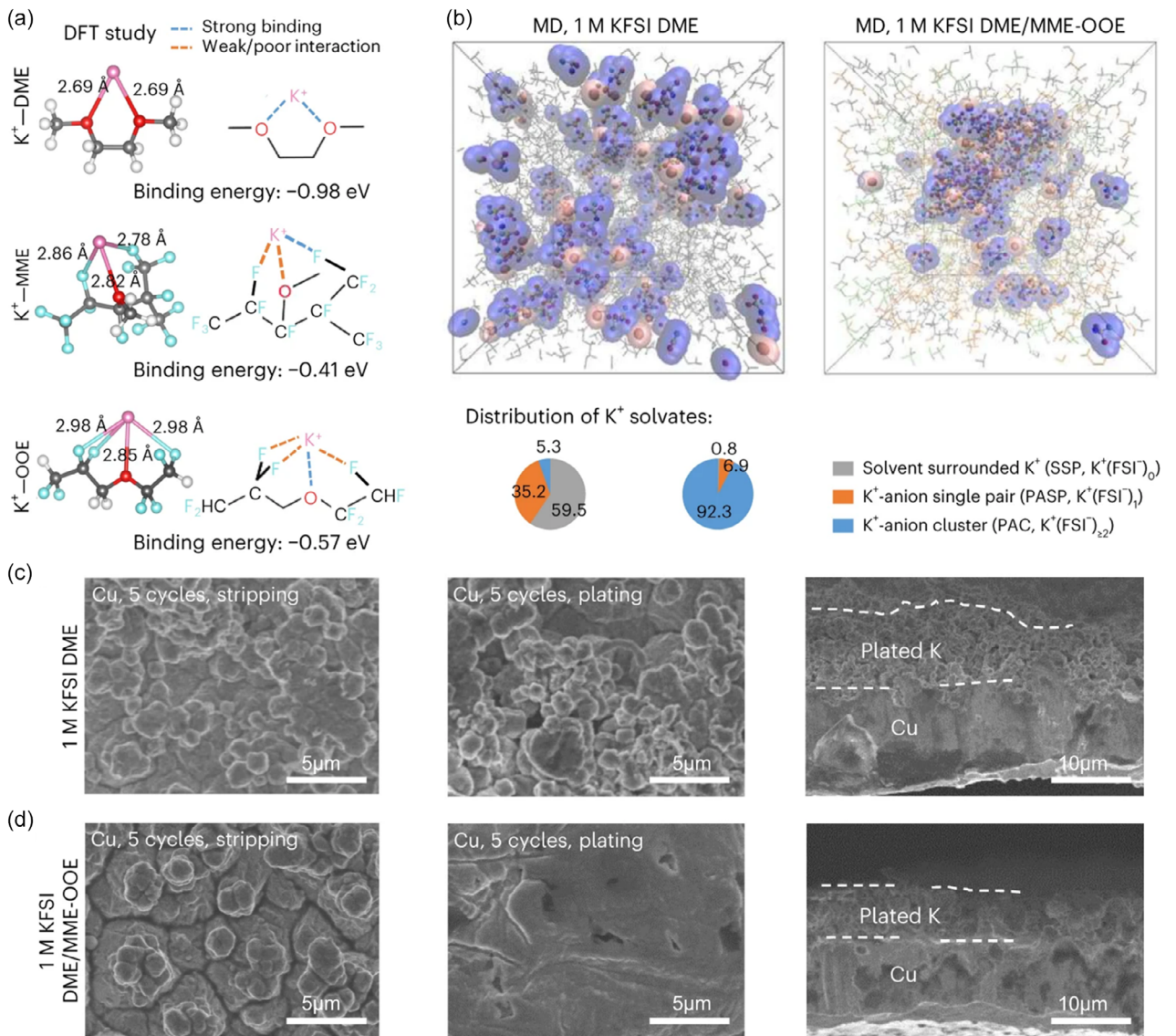


Figure 11. Application of LHCE in KMBs. a) Calculations of coordination structure and binding energy of K⁺ with solvent and diluent molecules by DFT. b) MD simulations demonstrating the solvation structures of K⁺ in 1 M KFSI/DME and 1 M KFSI/DME-MME-OOE electrolytes. c,d) SEM images depicting the top and cross section of electrochemically stripped and plated K metal on Cu electrodes using different electrolytes. Reproduced with permission.^[132] Copyright 2024, The Author(s).

broadening the electrochemical window of the electrolyte to over 5.1 V while preserving potassium salt solubility.^[106] The K||Cu cell assembled with this strategy exhibited exceptional cycling stability, achieving an average CE of 98.4% over 200 cycles, while the K||PB cell demonstrated stable cycling for over 700 cycles at a cutoff voltage of 4.5 V. Furthermore, Yang et al. observed a similar cosolvent synergy in the 1,2-diethoxyethane (DEE) and DBE solvents system, further validating the universality of this strategy.^[107] Therefore, for LHCE systems in KIBs, the utilization of weakly coordinated solvents or cosolvents rather than traditional diluents represents a promising research direction.

From the perspective of solvation, there exists a competitive interaction between solvents and anions with cations in the electrolyte. Due to the significantly larger ionic radius of K⁺ compared to Li⁺ and Na⁺, its charge density is substantially lower than that of the latter two ions. This fundamental characteristic results in

inherently weaker interactions between K⁺ and solvent molecules relative to Li⁺ and Na⁺. Such properties provide favorable conditions for the realization of WSEs. The WSEs significantly attenuate cation-solvent interactions while simultaneously enhancing cation-anion interactions. This unique characteristic facilitates the formation of anion-derived inorganic-rich SEIs even at moderate concentrations. However, the extremely weak coordination between weakly solvating solvents and K⁺ significantly reduces the dissociation of potassium salts, resulting in generally lower ionic conductivity in WSEs systems. Furthermore, due to the high reactivity of K metal, the current application of WSEs in KMBs is primarily limited to phosphate-based and ether-based solvents.

Phosphate-based solvents have gained widespread application in battery technologies due to their inherent nonflammability (Figure 12b).^[108,109] However, traditional phosphate-based electrolytes suffer from significant drawbacks, including low CE

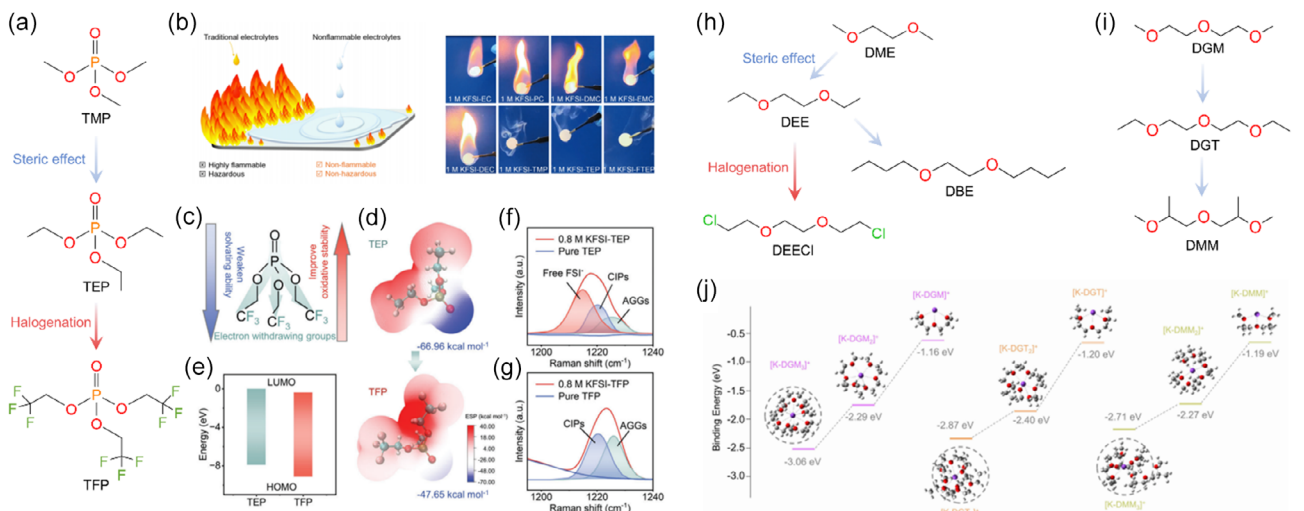


Figure 12. Strategic design approaches for WSEs. a) Molecular structures of representative phosphate-based electrolyte solvents, including TMP, TEP, and TFP, employed in battery systems. b) Comparative analysis of safety characteristics among carbonate-based, ether-based, and phosphate-based electrolytes. Reproduced with permission.^[104] Copyright 2023, The Royal Society of Chemistry. c) Fundamental design principles for developing fluorinated phosphate-based solvents. d) ESP mapping results for TEP and TFP molecules. e) Energy-level alignments of the LUMO and HOMO for TEP and TFP solvent molecules. f,g) Raman spectra analysis of different electrolytes. Reproduced with permission.^[111] Copyright 2023, Wiley-VCH GmbH. h,i) Molecular architectures of typical ether-based solvents, including DME, DEE, DBE, DEECl, DGM, DGT, and DMM. j) Comparative analysis of binding energies between K^+ and various solvent molecules with different solvation structures. Reproduced with permission.^[114] Copyright 2023, Wiley-VCH GmbH.

and poor cycling stability. Through rational design of solvent molecules, the electrochemical performance of phosphate-based electrolytes in KMBs can be effectively improved (Figure 12a). For example, in the TMP solvent, it is necessary to increase the KFSI salt concentration ($>3\text{ M}$) to enhance the compatibility between the electrolyte and K metal.^[110] By increasing the end-group chain length of TMP solvent molecules, the resulting TEP solvent demonstrates significantly enhanced compatibility with K metal. In the 2 M KFSI/TEP electrolyte, the $K||Cu$ asymmetric cells achieve an average CE of up to 99.6%.^[111] To further optimize the solvation structure of phosphate-based electrolytes, selective incorporation of $-CF_3$ onto the phosphate-based backbones can be implemented (Figure 12c).^[112,113] Using DFT calculations, the electrostatic potential (ESP) and LUMO–HOMO energy levels of TEP and tris(2,2,2-trifluoroethyl) phosphate (TFP) solvent molecules were analyzed, revealing the significant impact of F atom incorporation on molecular properties (Figure 12d,e). Compared to TEP solvent molecule, the functionalized TFP solvent molecule exhibits enhanced oxidative stability and weaker solvating ability. Raman spectra further confirm that the weak solvating ability of TFP solvent facilitates the formation of AGGs (Figure 12f,g). Electrochemical performance showed that the $K||Cu$ asymmetric cells using 1 M KFSI/TFP electrolyte demonstrated remarkable cycling stability, maintaining consistent operation for over 200 days. Furthermore, in terms of high-voltage stability, the $K||KVPO_4F$ full cell exhibited exceptional electrochemical performance in the TFP-based electrolyte, achieving an impressive oxidation stability of up to 4.95 V.

In ether-based electrolyte systems, despite exhibiting relatively sluggish chemical reactivity with K metal, the persistent challenge of K dendrite formation continues to significantly compromise both cycling performance and safety of the batteries. Consequently, it is imperative to strategically optimize the ether

solvent by advanced structural engineering approaches, aiming to refine the electrolyte's solvation structure and ultimately establish a robust and stable SEI layer. Recent advancements in molecular engineering of ether-based solvents have demonstrated remarkable progress in their application within KMBs. This innovative design paradigm is primarily accomplished through three strategic approaches: 1) implementation of steric hindrance effects, 2) strategic incorporation of halogen atoms, and 3) systematic optimization of molecular structure (Figure 12h,i).^[114–116]

Li et al. strategically employed steric hindrance effects to modulate the solvation structure of K^+ .^[116] By systematic substitution of methoxy groups in DME with larger ethoxy groups, they obtained DEE which exhibits weaker solvation capacity. This innovative design led to remarkable electrochemical performance in $K||Cu$ asymmetric cells. Specifically, the $K||Cu$ asymmetric cells achieved an average CE of 98.1% after 100 cycles in the 1 M KFSI/DEE electrolyte, while maintaining an impressive 98.8% average CE after 550 cycles in the 2 M KFSI/DEE electrolyte. Through enhancement of steric hindrance effects, the obtained DBE demonstrates remarkable potassium salt dissolution inhibition characteristics.^[106] Hu et al. advanced the molecular design of DEE by incorporating an electron-withdrawing chloro (Cl)-substitution group, resulting in the development of 1,2-bis(2-chloroethoxy) ethane (DEECl) as a new electrolyte solvent.^[114] This Cl-functionalized ether-based electrolyte demonstrated exceptional capability in promoting the formation of a homogeneous dual-halide-based SEI layer. Remarkably, even at a relatively low concentration of $\approx 0.91\text{ M}$ KFSI/DEECl electrolyte, the $K||Cu$ asymmetric cells maintained excellent cycling stability, achieving a high average CE of 98.3% after 400 cycles. Furthermore, Ma et al. systematically engineered the molecular structure of DGM by two optimizations of molecular structure strategies: 1) expansion of terminal methyl groups ($-CH_3$) to ethyl groups ($-CH_2CH_3$), yielding

diethylene glycol diethyl ether (DGT), and 2) incorporation of methyl groups ($-\text{CH}_3$) into the central molecular framework, resulting in dipropylene glycol dimethyl ether (DMM) (Figure 12i).^[115] Computational analyses revealed a significantly reduced binding energy between K^+ and DMM molecule compared to both DGM and DGT molecules, suggesting lower solvation ability between DMM solvent and K^+ (Figure 12j). Electrochemical characterization demonstrated superior compatibility of the DMM-based electrolyte with K metal anodes compared to the DGT- and DGM-based electrolytes, highlighting the critical role of molecular structure in electrolyte optimization.

Furthermore, significant progress has been made in the research of carbonate-based WSEs. Heng et al. developed a fluorinated solvent-based weakly solvating electrolyte system for high-voltage KMBs.^[117] This system utilizes low dielectric constant solvents, 2,2,2-trifluoroethyl carbonate (FEMC) and fluoroethylene carbonate (FEC), whose weak K^+ coordination capability significantly enhances anion–cation interactions. The designed 1 M KFSI/FEMC-FEC electrolyte enables stable cycling of the $\text{K}||\text{KVOP}$ cell for over 600 cycles at an ultrahigh cutoff voltage of 4.95 V, demonstrating exceptional high-voltage compatibility. However, this fluorinated system exhibits poor compatibility with K metal anodes compared to ether-based solvents, the Aurbach tests on $\text{K}||\text{Al}$ asymmetric cell show a CE of only 94.42%, while $\text{K}||\text{K}$ symmetric cells display a significantly increased polarization voltage compared to conventional carbonate-based electrolytes.

4.2. Ionic Liquids

Ionic liquids (ILs), as a class of room-temperature molten salts with unique ionic coordination structures, have emerged as novel electrolyte functional materials due to their designable molecular configurations.^[118–120] Their molecular architecture is formed through between bulky organic cations and weakly coordinating anions. This special ionic association structure endows ILs with intrinsic nonflammability, a wide electrochemical stability window, and high thermal decomposition temperatures. As a key component of KIBs electrolytes, ILs can overcome the safety–performance trade-off dilemma of traditional organic electrolytes. Currently, research and development of ILs for KIBs are in their early stages.

Yoshii et al. were the first to successfully apply ILs in KMBs.^[121] The IL they developed consists of 0.5 M KTFSI and 1-methyl-1-propylpyrrolidinium TFSI (Py13TFSI), exhibiting an ionic conductivity of 2.1 mS cm^{-1} at 25°C . This IL enabled reversible K metal plating/stripping at an extremely low current density ($6.4 \mu\text{A cm}^{-2}$), and the $\text{K}||\text{K}_2\text{Ni}_{2-x}\text{Co}_x\text{TeO}_6$ cell delivered a specific capacity of only $16\text{--}38 \text{ mAh g}^{-1}$ at a rate of 0.05 C ($\approx 6.4 \text{ mA g}^{-1}$). Cycling performance tests revealed that the $\text{K}||\text{K}_2\text{Ni}_{2-x}\text{Co}_x\text{TeO}_6$ cell retained 88% of its capacity after 100 cycles. Subsequently, Sun et al. developed an IL comprising 1-ethyl-3-methylimidazolium chloride ([EMIm]Cl)/ $\text{AlCl}_3/\text{KCl}/\text{KFSI}$, which demonstrated an ultrahigh ionic conductivity of 13.3 mS cm^{-1} at room temperature and supported stable cycling of a $\text{K}||\text{PB}@\text{rGO}$ cell for 800 cycles at a cutoff voltage of 4.5 V, with an average CE of 99.9%.^[122] The performance advantages stem from the robust passivation interface containing K,

Al, F, and Cl provided by this electrolyte, which is key to the exceptional battery cycling performance. Despite the excellent flame retardancy and electrochemical performance of ILs, the cost of ILs is relatively high compared to traditional organic solvents. Therefore, it is necessary to develop new ILs with affordable material costs.

4.3. Polymer Electrolytes

Currently, KMBs predominantly employ organic liquid electrolytes, which are prone to volatile leakage and flash ignition under thermal abuse conditions, posing significant safety hazards. The adoption of solid-state electrolytes as an alternative, by constructing solid media that integrate both ionic conduction and physical barrier functions, can fundamentally address the issues of electrolyte volatility and flammability.^[123,124] Current research primarily focuses on two systems: solid polymer electrolytes (SPEs) and gel polymer electrolytes (GPEs). However, both face critical challenges such as poor electrode/electrolyte interface compatibility and insufficient ionic conductivity at room temperature.^[125]

To address the aforementioned issues, researchers have developed composite solid-state electrolytes based on cellulose nonwoven fabrics. Feng et al. constructed a composite electrolyte with both thermal and chemical stability using a cellulose framework to support a polypropylene carbonate (PPC)-KFSI.^[126] This SPEs demonstrated high ionic conductivity at room temperature, making them suitable for practical applications. Lyu et al. proposed an iodinated SPE (ISPE) that achieved breakthrough performance through dual mechanisms: activating K^+ transport channels in polyethylene oxide (PEO) matrices and in situ a stable interlayer, effectively inhibiting K dendrite formation.^[127] This ISPE exhibited a high ionic conductivity of $3.25 \times 10^{-4} \text{ S cm}^{-1}$ at 50°C , with a K^+ transference number of 0.592 and an expanded electrochemical stability window of 5.2 V. Regarding GPEs optimization, Li et al. employed ultraviolet-initiated in situ polymerization technology to combine an ethoxylated trimethylpropane triacrylate (ETPTA) crosslinked network with low-concentration ether-based electrolytes.^[128] This approach produced high-performance quasisolid crosslinked GPEs that overcome the drawbacks of electrolyte leakage and high flammability.

5. Summary and Outlook

KMBs demonstrate tremendous potential for practical applications, yet they face significant challenges, including K dendrite formation, interface instability, and volumetric expansion during cycling. To address these critical issues, researchers have proposed various innovative optimization strategies. First, the primary optimization strategy involves the rational design of K metal host materials, which serves to enhance K^+ reactivity and reduce local current density, thereby effectively suppressing K dendrite growth. Second, the construction of ASEI layers improves interface stability and enhances ion transport efficiency. Furthermore, the modification of current collector structural design and developing novel functional separators play crucial

roles in inhibiting K dendrite growth and improving battery performance. Finally, by precisely regulating electrolyte composition and concentration, more stable SEI layers can be formed, substantially extending battery cycle life. Despite remarkable progress, further in-depth research is still required in areas such as battery safety enhancement and cost reduction before achieving commercial viability of KMBs. Based on current research advancements, we propose several key research directions to facilitate the development of high-performance K metal anodes.

5.1. Innovative Development of K Metal Host Materials

Despite significant advancements in the development and application of diverse K metal host materials, several critical limitations persist. These challenges primarily include: 1) inadequate potassiphilicity in certain materials, resulting in nonuniform K metal deposition, coupled with the complexity and high cost associated with conventional potassiphilicity enhancement methods; 2) insufficient electrical conductivity, which compromises electron transfer efficiency; and 3) structural degradation during prolonged cycling. To address these issues, future research directions should focus on the exploration of innovative nanostructured materials, advanced composite systems, and specially engineered surface modifications. These approaches aim to simultaneously enhance three key characteristics: potassiphilicity, electrical conductivity, and structural stability of host materials. Such advancements would facilitate uniform K metal deposition and efficient ion/electron transport, ultimately leading to significant improvements in cycle stability and rate capability of KMBs.

5.2. Optimized Design of ASEI

ASEI plays a crucial role in protecting K metal anodes; however, current SEI construction strategies still exhibit several critical limitations. These include insufficient interface uniformity, inadequate denseness, and compromised stability, all of which require substantial improvement. Future research directions should focus on precise control of SEI composition and architecture through strategic incorporation of inorganic components to enhance structural stability, coupled with optimization of organic constituents to improve interface flexibility. Such dual-component engineering would enable the SEI layer to better accommodate the substantial volume fluctuations of K metal during charge/discharge process, effectively suppress K dendrite formation, and significantly extend battery cycle life.

5.3. Synergistic Improvement of Current Collectors and Separator Materials

The performance characteristics of current collectors and separator materials exert a profound influence on the overall electrochemical behavior of KMBs. Concerning current collector optimization, beyond the fundamental enhancement of electrical conductivity and mechanical robustness, advanced strategies

should focus on developing engineered surface architectures and functional coatings. These modifications aim to precisely regulate K metal deposition uniformity and effectively mitigate dendrite formation. In the development of novel separator materials, systematic evaluation of conventional performance parameters (microstructural characteristics, mechanical integrity, and thermal stability) should be complemented by particular emphasis on optimizing the areal density and volumetric parameters. These parameters serve as critical determinants of the gravimetric energy density and volumetric energy density in advanced battery systems.

5.4. Diversification and Refined Control of Electrolytes

The composition and physicochemical properties of electrolytes play a pivotal role in determining the electrochemical performance of KMBs. Future research directions should focus on two complementary strategies: 1) expanding the electrolyte chemical space through exploration of novel potassium salt–solvent combinations to achieve enhanced ionic conductivity, superior chemical stability, and wide electrochemical stability windows and 2) implementing precise control over electrolyte parameters, including concentration optimization, strategic additive incorporation, and tailored solvation structure design. These approaches aim to synergistically optimize SEI formation and K metal deposition behavior, ultimately enabling the development of high-performance KMBs.

5.5. ILs and Polymer Electrolytes

In KMBs, research on ILs remains in its nascent stages. To achieve targeted design and performance optimization of ILs, priority should be given to establishing a comprehensive evaluation framework that balances electrochemical characteristics with scale production costs. The development of solid-state electrolytes combining superior electrochemical performance with economic viability also represents a critical breakthrough challenge. Although solid-state electrolytes inherently eliminate the need for separator components, they still face two major technical bottlenecks: electrode–electrolyte interfacial compatibility issues and challenges in scalable manufacturing processes. Surface modification of solid-state electrolytes through interface engineering strategies is poised to emerge as a pivotal research direction in advancing this field.

In conclusion, the development of K metal anodes for KMBs presents substantial opportunities for scientific advancement and technological innovation. Through sustained and systematic research efforts, it is anticipated that the current technical challenges can be effectively addressed, leading to the realization of KMBs with superior performance characteristics, extended cycle life, and competitive cost-effectiveness. These advancements are expected to make significant contributions to the evolution of next-generation energy storage systems, thereby addressing the growing global demand for efficient and sustainable energy storage solutions.

Acknowledgements

Y.C. and J.W. contributed equally to this work. This work was supported by the National Natural Science Foundation of China (grant nos. 52372189 and U20A20247) and the Science and Technology Innovation Program of Hunan Province (2023RC3109).

Conflict of Interest

The authors declare no conflict of interest.

Keywords: anode host materials · artificial solid-electrolyte interfaces · current collector modifications · electrolyte optimizations · separator designs

- [1] Z. Yang, J. Zhang, M. C. Kintner-Meyer, X. Lu, D. Choi, J. P. Lemmon, J. Liu, *Chem. Rev.* **2011**, *111*, 3577.
- [2] T. Hosaka, K. Kubota, A. S. Hameed, S. Komaba, *Chem. Rev.* **2020**, *120*, 6358.
- [3] M. Ma, S. Chong, K. Yao, H. K. Liu, S. X. Dou, W. Huang, *Matter* **2023**, *6*, 3220.
- [4] Z. Li, K. Zhu, P. Liu, L. Jiao, *Adv. Energy Mater.* **2021**, *12*, 2100359.
- [5] X. Min, J. Xiao, M. Fang, W. Wang, Y. Zhao, Y. Liu, A. M. Abdelkader, K. Xi, R. V. Kumar, Z. Huang, *Energy Environ. Sci.* **2021**, *14*, 2186.
- [6] M. Xia, J. Zhou, B. Lu, *Adv. Energy Mater.* **2024**, *15*, 2404032.
- [7] S. Chong, S. Qiao, X. Wei, T. Li, L. Yuan, S. Dong, W. Huang, *iScience* **2021**, *24*, 103494.
- [8] K. Lei, C. Wang, L. Liu, Y. Luo, C. Mu, F. Li, J. Chen, *Angew. Chem., Int. Ed.* **2018**, *57*, 4687.
- [9] Y. Liu, Y. X. Lu, Y. S. Xu, Q. S. Meng, J. C. Gao, Y. G. Sun, Y. S. Hu, B. B. Chang, C. T. Liu, A. M. Cao, *Adv. Mater.* **2020**, *32*, 2000505.
- [10] W. Zhang, J. Mao, S. Li, Z. Chen, Z. Guo, *J. Am. Chem. Soc.* **2017**, *139*, 3316.
- [11] J. Liu, L. Huang, H. Wang, L. Sha, M. Liu, Z. Sun, J. Gu, H. Liu, J. Zhao, Q. Zhang, L. Zhang, *Electrochem. Energy Rev.* **2024**, *7*, 34.
- [12] C. Yang, J. Feng, F. Lv, J. Zhou, C. Lin, K. Wang, Y. Zhang, Y. Yang, W. Wang, J. Li, S. Guo, *Adv. Mater.* **2018**, *30*, 1800036.
- [13] M. Ou, Y. Zhang, Y. Zhu, C. Fan, S. Sun, J. Feng, X. Sun, P. Wei, J. Xu, J. Peng, X. Wu, G. Jiang, Q. Li, C. Fang, J. Han, *ACS Appl. Mater. Interfaces* **2021**, *13*, 28261.
- [14] Y. Xu, C. Zhang, M. Zhou, Q. Fu, C. Zhao, M. Wu, Y. Lei, *Nat. Commun.* **2018**, *9*, 1720.
- [15] X. He, J. Liao, Z. Tang, L. Xiao, X. Ding, Q. Hu, Z. Wen, C. Chen, *J. Power Sources* **2018**, *396*, 533.
- [16] K. Lei, F. Li, C. Mu, J. Wang, Q. Zhao, C. Chen, J. Chen, *Energy Environ. Sci.* **2017**, *10*, 552.
- [17] R. Huang, J. Lin, J. Zhou, E. Fan, X. Zhang, R. Chen, F. Wu, L. Li, *Small* **2021**, *17*, 2007597.
- [18] D. Adekoya, H. Chen, H. Y. Hoh, T. Gould, M. S. J. T. Balogun, C. Lai, H. Zhao, S. Zhang, *ACS Nano* **2020**, *14*, 5027.
- [19] L. Fan, R. Ma, Q. Zhang, X. Jia, B. Lu, *Angew. Chem., Int. Ed.* **2019**, *58*, 10500.
- [20] J. Jiang, Z. Chen, Y. Chen, Q. Zhuang, Z. Ju, X. Zhang, *Adv. Funct. Mater.* **2024**, *34*, 2402416.
- [21] W. Jian, X. Qiu, Y. Lai, P. Yin, J. Lin, W. Zhang, *Adv. Energy Mater.* **2023**, *13*, 2301303.
- [22] J. Xu, S. Dou, Y. Wang, Q. Yuan, Y. Deng, Y. Chen, *Trans. Tianjin Univ.* **2021**, *27*, 248.
- [23] H. Gao, T. Zhou, Y. Zheng, Q. Zhang, Y. Liu, J. Chen, H. Liu, Z. Guo, *Adv. Funct. Mater.* **2017**, *27*, 1702634.
- [24] E. Zhang, X. Jia, B. Wang, J. Wang, X. Yu, B. Lu, *Adv. Sci.* **2020**, *7*, 2000470.
- [25] X. Du, Y. Gao, B. Zhang, *Adv. Funct. Mater.* **2021**, *31*, 2102562.
- [26] H. He, D. Huang, Q. Gan, J. Hao, S. Liu, Z. Wu, W. K. Pang, B. Johannessen, Y. Tang, J.-L. Luo, H. Wang, Z. Guo, *ACS Nano* **2019**, *13*, 11843.
- [27] J. Park, J. Lee, M. H. Alfarouqi, W.-J. Kwak, J. Kim, J.-Y. Hwang, *J. Mater. Chem. A* **2020**, *8*, 16718.
- [28] X.-C. Wang, L.-K. Zhao, Z.-M. Liu, Q. Gu, X.-W. Gao, W.-B. Luo, *ACS Energy Lett.* **2024**, *10*, 48.
- [29] W. Yao, K. Liao, T. Lai, H. Sul, A. Manthiram, *Chem. Rev.* **2024**, *124*, 4935.
- [30] L. Qin, L. Schkeryantz, J. Zheng, N. Xiao, Y. Wu, *J. Am. Chem. Soc.* **2020**, *142*, 11629.
- [31] T. Hosaka, S. Muratsubaki, K. Kubota, H. Onuma, S. Komaba, *J. Phys. Chem. Lett.* **2019**, *10*, 3296.
- [32] L. Wang, H. Wang, M. Cheng, Y. Hong, M. Li, H. Su, J. Sun, J. Wang, Y. Xu, *ACS Appl. Energy Mater.* **2021**, *4*, 6245.
- [33] G. Cheng, S. Liu, X. Wang, X. Li, Y. Su, J. Shi, M. Huang, Z. Shi, H. Wang, Z. Yan, *ACS Appl. Mater. Interfaces* **2022**, *14*, 45364.
- [34] Z. Sun, M. Liu, B. Liu, R. Khan, J. Zhao, L. Huang, Y. Wu, *ACS Appl. Mater. Interfaces* **2023**, *15*, 58429.
- [35] Y. Yang, C. Huang, Y. Zhang, Y. Wu, X. Zhao, Y. Qian, G. Chang, Q. Tang, A. Hu, X. Chen, *ACS Appl. Mater. Interfaces* **2022**, *14*, 55577.
- [36] M. Zhou, W. Qi, Z. Hu, M. Cheng, X. Zhao, P. Xiong, H. Su, M. Li, J. Hu, Y. Xu, *ACS Appl. Mater. Interfaces* **2021**, *13*, 17629.
- [37] S. Li, H. Zhu, C. Gu, F. Ma, W. Zhong, M. Liu, H. Zhang, Z. Zeng, S. Cheng, J. Xie, *ACS Energy Lett.* **2023**, *8*, 3467.
- [38] J. Park, Y. Jeong, M. H. Alfarouqi, Y. Liu, X. Xu, S. Xiong, M.-G. Jung, H.-G. Jung, J. Kim, J.-Y. Hwang, Y.-K. Sun, *ACS Energy Lett.* **2021**, *7*, 401.
- [39] Z. Wang, J.-F. Wu, W. Zhou, Y. Mo, S. Chen, T. Zhou, W. Shen, B. Ren, P. Huang, J. Liu, *ACS Energy Lett.* **2024**, *9*, 4534.
- [40] Z. Chen, L. Wang, J. Zheng, Y. Huang, H. Huang, C. Li, Y. Shao, X. Wu, X. Rui, X. Tao, H. Yang, Y. Yu, *ACS Nano* **2024**, *18*, 8496.
- [41] J. Meng, H. Zhu, Z. Xiao, X. Zhang, C. Niu, Y. Liu, G. Jiang, X. Wang, F. Qiao, X. Hong, F. Liu, Q. Pang, L. Mai, *ACS Nano* **2022**, *16*, 7291.
- [42] J. Xie, Y. Ji, L. Ma, Z. Wen, J. Pu, L. Wang, S. Ding, Z. Shen, Y. Liu, J. Li, W. Mai, G. Hong, *ACS Nano* **2023**, *17*, 1511.
- [43] M. Ye, J. Y. Hwang, Y. K. Sun, *ACS Nano* **2019**, *13*, 9306.
- [44] X. Tang, D. Zhou, P. Li, X. Guo, B. Sun, H. Liu, K. Yan, Y. Gogotsi, G. Wang, *Adv. Mater.* **2020**, *32*, e1906739.
- [45] L. Qin, Y. Lei, H. Wang, J. Dong, Y. Wu, D. Zhai, F. Kang, Y. Tao, Q. H. Yang, *Adv. Energy Mater.* **2019**, *9*, 1901427.
- [46] P. Shi, S. Zhang, G. Lu, L. Wang, Y. Jiang, F. Liu, Y. Yao, H. Yang, M. Ma, S. Ye, X. Tao, Y. Feng, X. Wu, X. Rui, Y. Yu, *Adv. Energy Mater.* **2020**, *11*, 2003381.
- [47] H. Wang, J. Hu, J. Dong, K. C. Lau, L. Qin, Y. Lei, B. Li, D. Zhai, Y. Wu, F. Kang, *Adv. Energy Mater.* **2019**, *9*, 1902697.
- [48] D. Zhang, M. Liu, W. Shi, Y. Qiu, Y. Hu, Z. Yuan, H. Xue, L. Kong, K. Zhao, J. Ren, B. Liu, *Adv. Energy Mater.* **2024**, *14*, 2401960.
- [49] D. Zhang, X. Ma, L. Wu, J. Wen, F. Li, J. Zhou, A. M. Rao, B. Lu, *Adv. Energy Mater.* **2022**, *13*, 2203277.
- [50] F. Liu, L. Wang, F. Ling, X. Zhou, Y. Jiang, Y. Yao, H. Yang, Y. Shao, X. Wu, X. Rui, C. He, Y. Yu, *Adv. Funct. Mater.* **2022**, *32*, 2210166.
- [51] N. Ren, L. Wang, X. Li, K. Cao, Z. He, Y. Shao, J. Xiao, Y. Zhu, B. Pan, S. Jiao, C. Chen, *Adv. Funct. Mater.* **2024**, *34*, 2313538.
- [52] S. Xie, W. Xie, Q. Zhang, X. Cheng, X. Ouyang, B. Lu, *Adv. Funct. Mater.* **2023**, *33*, 2302880.
- [53] L. K. Zhao, X. W. Gao, J. Mu, W. B. Luo, Z. Liu, Z. Sun, Q. F. Gu, F. Li, *Adv. Funct. Mater.* **2023**, *33*, 2304292.
- [54] J. L. Zhou, L. K. Zhao, Y. Lu, X. W. Gao, Y. Chen, Z. M. Liu, Q. F. Gu, W. B. Luo, *Adv. Funct. Mater.* **2024**, *34*, 2403754.
- [55] Y. Jiang, Y. Yang, F. Ling, G. Lu, F. Huang, X. Tao, S. Wu, X. Cheng, F. Liu, D. Li, H. Yang, Y. Yao, P. Shi, Q. Chen, X. Rui, Y. Yu, *Adv. Mater.* **2022**, *34*, 2109439.
- [56] P. Liu, Y. Wang, H. Hao, S. Basu, X. Feng, Y. Xu, J. A. Boscoboinik, J. Nanda, J. Watt, D. Mitlin, *Adv. Mater.* **2020**, *32*, 2070365.
- [57] H. Yang, F. He, M. Li, F. Huang, Z. Chen, P. Shi, F. Liu, Y. Jiang, L. He, M. Gu, Y. Yu, *Adv. Mater.* **2021**, *33*, 2106353.
- [58] Y. Zhao, B. Liu, Y. Yi, X. Lian, M. Wang, S. Li, X. Yang, J. Sun, *Adv. Mater.* **2022**, *34*, 2202902.
- [59] S. Wang, Y. Yan, D. Xiong, G. Li, Y. Wang, F. Chen, S. Chen, B. Tian, Y. Shi, *Angew. Chem., Int. Ed.* **2021**, *60*, 25122.
- [60] R. Zhou, H. Tan, Y. Gao, Z. Hou, X. Du, B. Zhang, *Carbon* **2022**, *186*, 141.
- [61] X. Li, J. Sun, L. Song, X. Jiang, X. Mo, J. Shen, X. Zhou, *Chem. Eng. J.* **2024**, *490*, 151521.
- [62] J. Xiong, M. Ye, Z. Wang, J. Chen, Y. Zhang, Y. Tang, C. C. Li, *Chem. Eng. J.* **2022**, *442*, 135927.
- [63] D.-T. Zhang, M.-C. Liu, M.-P. Li, Z.-Z. Yuan, Y.-X. Hu, H. Chen, C.-Y. Li, L.-B. Kong, K. Zhao, J.-Q. Ren, B. Liu, *Chem. Eng. J.* **2024**, *482*, 148896.
- [64] Z. Li, L. Ma, K. Han, Y. Ji, J. Xie, L. Pan, J. Li, W. Mai, *Chem. Sci.* **2023**, *14*, 9114.
- [65] Z. Cui, J. Song, M. Chen, W. Wang, W. Zhang, Q. Zhu, *Energy Storage Mater.* **2024**, *71*, 103649.
- [66] P. Li, T. Xu, P. Ding, J. Deng, C. Zha, Y. Wu, Y. Wang, Y. Li, *Energy Storage Mater.* **2018**, *15*, 8.
- [67] J. Zhang, Y. Li, L. Zhu, X. Wang, J. Tu, *Energy Storage Mater.* **2021**, *41*, 606.
- [68] L.-K. Zhao, X.-W. Gao, Q. Gu, X. Ge, Z. Ding, Z. Liu, W.-B. Luo, *eScience* **2024**, *4*, 100201.

- [69] G. Cheng, S. Liu, Y. Su, X. Wang, X. Li, J. Shi, M. Huang, Z. Shi, H. Wang, *J. Alloys Compd.* **2022**, *913*, 165329.
- [70] D.-T. Zhang, W.-J. Shi, M.-P. Li, H. Chen, C.-Y. Li, Y.-X. Hu, L.-B. Kong, K. Zhao, J.-Q. Ren, H.-T. Xue, Z.-Z. Yuan, M.-C. Liu, *J. Energy Storage* **2024**, *77*, 109903.
- [71] J. Qi, C. Lin, S. Deng, Y. Zuo, H. Zheng, X. Jiao, W. Yan, J. Zhang, *J. Mater. Chem. A* **2024**, *12*, 6968.
- [72] F. Qiao, J. Meng, J. Wang, P. Wu, D. Xu, Q. An, X. Wang, L. Mai, *J. Mater. Chem. A* **2021**, *9*, 23046.
- [73] D.-T. Zhang, M.-C. Liu, M.-P. Li, H. Chen, C.-Y. Li, Y.-X. Hu, L.-B. Kong, X.-Y. Zhang, B.-N. Gu, M.-J. Liu, K. Zhao, J.-Q. Ren, Z.-Z. Yuan, Y.-L. Chueh, *J. Mater. Chem. A* **2023**, *11*, 20741.
- [74] Y. Li, L. Zhang, S. Liu, X. Wang, D. Xie, X. Xia, C. Gu, J. Tu, *Nano Energy* **2019**, *62*, 367.
- [75] J. Wang, W. Yan, J. Zhang, *Nano Energy* **2022**, *96*, 107131.
- [76] J. Wang, J. Yuan, C. Chen, L. Wang, Z. Zhai, Q. Fu, Y. Liu, L. Dong, W. Yan, A. Li, J. Zhang, *Nano Energy* **2020**, *75*, 104914.
- [77] H. Shi, Y. Dong, S. Zheng, C. Dong, Z.-S. Wu, *Nanoscale Adv.* **2020**, *2*, 4212.
- [78] S. Li, H. Zhu, Y. Liu, Z. Han, L. Peng, S. Li, C. Yu, S. Cheng, J. Xie, *Nat. Commun.* **2022**, *13*, 4911.
- [79] H. Ding, J. Wang, J. Zhou, C. Wang, B. Lu, *Nat. Commun.* **2023**, *14*, 2305.
- [80] C. Qin, D. Wang, Y. Liu, P. Yang, T. Xie, L. Huang, H. Zou, G. Li, Y. Wu, *Nat. Commun.* **2021**, *12*, 7184.
- [81] H. Jiang, X. Lin, C. Wei, J. Feng, X. Tian, *Small* **2021**, *18*, 2104264.
- [82] J. Sun, L. Duan, Z. Yuan, X. Li, D. Yan, X. Zhou, *Small* **2024**, *20*, 2311314.
- [83] M. Ma, K. Yao, Y. Wang, D. Fattakhova-Rohlfing, S. Chong, *Adv. Funct. Mater.* **2024**, *34*, 2315662.
- [84] J. Sun, Y. Du, Y. Liu, D. Yan, X. Li, D. H. Kim, Z. Lin, X. Zhou, *Chem. Soc. Rev.* **2025**, *54*, 2543.
- [85] Y. Yang, G. Qu, Z. Wei, T. Hu, Y. Hu, Z. Wei, F. Mo, H. Li, G. Liang, *Adv. Funct. Mater.* **2024**, *34*, 2409950.
- [86] W. Liu, P. Liu, D. Mitlin, *Adv. Energy Mater.* **2020**, *10*, 2070177.
- [87] L. Song, R. Li, W. Liao, J. Sun, X. Li, Y. Xu, G. Zhou, X. Zhou, *Energy Storage Mater.* **2024**, *71*, 103643.
- [88] W. Deng, Z. Yu, H. Yang, Z. Chen, J. Zheng, Z. He, Y. Shao, S. Jiao, X. Tao, Y. Shen, X. Yu, Y. Yu, *Adv. Mater.* **2024**, *36*, 2412446.
- [89] P. Liu, H. Hao, H. Celio, J. Cui, M. Ren, Y. Wang, H. Dong, A. R. Chowdhury, T. Hutter, F. A. Perras, J. Nanda, J. Watt, D. Mitlin, *Adv. Mater.* **2022**, *34*, 2105855.
- [90] T. Wang, Q. Liu, J. Zhou, X. Wang, B. Lu, *Adv. Energy Mater.* **2022**, *12*, 2202357.
- [91] Y. Yang, G. Qu, H. Wei, Z. Wei, C. Liu, Y. Lin, X. Li, C. Han, C. Zhi, H. Li, *Adv. Energy Mater.* **2023**, *13*, 2203729.
- [92] Y. Yamada, J. Wang, S. Ko, E. Watanabe, A. Yamada, *Nat. Energy* **2019**, *4*, 269.
- [93] J. Wen, H. Fu, D. Zhang, X. Ma, L. Wu, L. Fan, X. Yu, J. Zhou, B. Lu, *ACS Nano* **2023**, *17*, 16135.
- [94] T. Hosaka, K. Kubota, H. Kojima, S. Komaba, *Chem. Commun.* **2018**, *54*, 8387.
- [95] J. Zhang, T. Liu, X. Cheng, M. Xia, R. Zheng, N. Peng, H. Yu, M. Shui, J. Shu, *Nano Energy* **2019**, *60*, 340.
- [96] Y. Hu, L. Fan, A. M. Rao, W. Yu, C. Zhuoma, Y. Feng, Z. Qin, J. Zhou, B. Lu, *Natl. Sci. Rev.* **2022**, *9*, nwac134.
- [97] P. Peljo, H. H. Girault, *Energy Environ. Sci.* **2018**, *11*, 2306.
- [98] B. Li, J. Zhao, Z. Zhang, C. Zhao, P. Sun, P. Bai, J. Yang, Z. Zhou, Y. Xu, *Adv. Funct. Mater.* **2018**, *29*, 1807137.
- [99] N. Xiao, W. D. McCulloch, Y. Wu, *J. Am. Chem. Soc.* **2017**, *139*, 9475.
- [100] S. Jiao, X. Ren, R. Cao, M. H. Engelhard, Y. Liu, D. Hu, D. Mei, J. Zheng, W. Zhao, Q. Li, N. Liu, B. D. Adams, C. Ma, J. Liu, J.-G. Zhang, W. Xu, *Nat. Energy* **2018**, *3*, 739.
- [101] W. Xu, H. Wang, J. Hu, H. Zhang, B. Zhang, F. Kang, D. Zhai, *Chem. Commun.* **2021**, *57*, 1034.
- [102] C. M. Efaw, Q. Wu, N. Gao, Y. Zhang, H. Zhu, K. Gering, M. F. Hurley, H. Xiong, E. Hu, X. Cao, W. Xu, J.-G. Zhang, E. J. Dufek, J. Xiao, X.-Q. Yang, J. Liu, Y. Qi, B. Li, *Nat. Mater.* **2023**, *22*, 1531.
- [103] X. Yi, H. Fu, A. M. Rao, Y. Zhang, J. Zhou, C. Wang, B. Lu, *Nat. Sustain.* **2024**, *7*, 326.
- [104] Z. Yuan, J. Liao, L. Song, A. Chen, J. Su, J. Wang, X. Zhou, *Angew. Chem., Int. Ed.* **2025**, *64*, e202415923.
- [105] Z. Piao, X. Wu, H.-R. Ren, G. Lu, R. Gao, G. Zhou, H.-M. Cheng, *J. Am. Chem. Soc.* **2023**, *145*, 24260.
- [106] M. Shen, Z. Dai, L. Fan, H. Fu, Y. Geng, J. Guan, F. Sun, A. M. Rao, J. Zhou, B. Lu, *Natl. Sci. Rev.* **2024**, *11*, nwae359.
- [107] Q. Yang, X. Zhou, T. Huang, Z. Chen, Y. Zhang, S. Shi, W. Zhang, L. Li, J. Wang, S. Dou, K. Lei, S. Zheng, *Angew. Chem., Int. Ed.* **2024**, *64*, e202422259.
- [108] J. Wang, Y. Yamada, K. Sodeyama, E. Watanabe, K. Takada, Y. Tateyama, A. Yamada, *Nat. Energy* **2017**, *3*, 22.
- [109] H. Wang, L. Nie, X. Chu, H. Chen, R. Chen, T. Huang, Q. Lai, J. Zheng, *Small Methods* **2023**, *8*, 2301104.
- [110] S. Liu, J. Mao, L. Zhang, W. K. Pang, A. Du, Z. Guo, *Adv. Mater.* **2021**, *33*, 2006313.
- [111] S. Liu, J. Mao, Q. Zhang, Z. Wang, W. K. Pang, L. Zhang, A. Du, V. Sencadas, W. Zhang, Z. Guo, *Angew. Chem., Int. Ed.* **2020**, *59*, 3638.
- [112] L. Fan, H. Xie, Y. Hu, Z. Caixiang, A. M. Rao, J. Zhou, B. Lu, *Energy Environ. Sci.* **2023**, *16*, 305.
- [113] Y. Gao, W. Li, B. Ou, S. Zhang, H. Wang, J. Hu, F. Kang, D. Zhai, *Adv. Funct. Mater.* **2023**, *33*, 2305829.
- [114] Y. Hu, H. Fu, Y. Geng, X. Yang, L. Fan, J. Zhou, B. Lu, *Angew. Chem., Int. Ed.* **2024**, *63*, e202403269.
- [115] X. Ma, H. Fu, J. Shen, D. Zhang, J. Zhou, C. Tong, A. M. Rao, J. Zhou, L. Fan, B. Lu, *Angew. Chem., Int. Ed.* **2023**, *62*, e202312973.
- [116] J. Li, Y. Hu, H. Xie, J. Peng, L. Fan, J. Zhou, B. Lu, *Angew. Chem., Int. Ed.* **2022**, *61*, 202208291.
- [117] Y. L. Heng, Z. Y. Gu, H. H. Liu, H. J. Liang, Y. Deng, J. Zhao, X. T. Wang, Z. H. Xue, H. Y. Lü, X. L. Wu, *Angew. Chem., Int. Ed.* **2025**, <https://doi.org/10.1002/anie.202423044>.
- [118] H. Onuma, K. Kubota, S. Muratsubaki, T. Hosaka, R. Tatara, T. Yamamoto, K. Matsumoto, T. Nohira, R. Hagiwara, H. Oji, S. Yasuno, S. Komaba, *ACS Energy Lett.* **2020**, *5*, 2849.
- [119] R. M. de Souza, L. J. A. de Siqueira, M. Karttunen, L. G. Dias, *J. Chem. Inf. Model.* **2019**, *60*, 485.
- [120] K. Beltrop, S. Beuker, A. Heckmann, M. Winter, T. Placke, *Energy Environ. Sci.* **2017**, *10*, 2090.
- [121] K. Yoshii, T. Masese, M. Kato, K. Kubota, H. Senoh, M. Shikano, *ChemElectroChem* **2019**, *6*, 3901.
- [122] H. Sun, P. Liang, G. Zhu, W. H. Hung, Y.-Y. Li, H.-C. Tai, C.-L. Huang, J. Li, Y. Meng, M. Angell, C.-A. Wang, H. Dai, *Proc. Natl. Acad. Sci.* **2020**, *117*, 27847.
- [123] W. Lyu, H. Fu, A. M. Rao, Z. Lu, X. Yu, Y. Lin, J. Zhou, B. Lu, *Sci. Adv.* **2024**, *10*, adr9602.
- [124] H. Gao, L. Xue, S. Xin, J. B. Goodenough, *Angew. Chem., Int. Ed.* **2018**, *57*, 5449.
- [125] X. Hu, Z. Zhang, X. Zhang, Y. Wang, X. Yang, X. Wang, M. Fayenagreenstein, H. A. Yehezkel, S. Langford, D. Zhou, B. Li, G. Wang, D. Aurbach, *Nat. Rev. Mater.* **2024**, *9*, 305.
- [126] H. Fei, Y. Liu, Y. An, X. Xu, G. Zeng, Y. Tian, L. Ci, B. Xi, S. Xiong, J. Feng, *J. Power Sources* **2018**, *399*, 294.
- [127] W. Lyu, X. Yu, Y. Lv, A. M. Rao, J. Zhou, B. Lu, *Adv. Mater.* **2024**, *36*, 2305795.
- [128] J. Li, H. Fu, M. Gu, J. Chen, J. Zhou, L. Fan, B. Lu, *Nano Lett.* **2024**, *24*, 11419.
- [129] P. Liu, Y. Wang, Q. Gu, J. Nanda, J. Watt, D. Mitlin, *Adv. Mater.* **2019**, *32*, 2070053.
- [130] Y. Gao, Z. Hou, R. Zhou, D. Wang, X. Guo, Y. Zhu, B. Zhang, *Adv. Funct. Mater.* **2022**, *32*, 2112399.
- [131] S. Lee, H. Park, J. Rizell, U. H. Kim, Y. Liu, X. Xu, S. Xiong, A. Matic, A. T. Zikri, H. Kang, Y. K. Sun, J. Kim, J. Y. Hwang, *Adv. Funct. Mater.* **2022**, *32*, 2209145.
- [132] D. Zhang, H. Fu, X. Ma, X. Yu, F. Li, J. Zhou, B. Lu, *Angew. Chem., Int. Ed.* **2024**, *63*, e202405153.
- [133] Y. Feng, A. M. Rao, J. Zhou, B. Lu, *Adv. Mater.* **2023**, *35*, 2300886.
- [134] P. Gao, F. Zhang, X. Wang, M. Wu, Q. Xiang, A. Yang, Y. Sun, J. Guo, Y. Huang, *ACS Nano* **2023**, *17*, 20325.
- [135] W. Chen, D. Zhang, H. Fu, J. Li, X. Yu, J. Zhou, B. Lu, *ACS Nano* **2024**, *18*, 12512.
- [136] M. Gu, X. Zhou, Q. Yang, S. Chu, L. Li, J. Li, Y. Zhao, X. Hu, S. Shi, Z. Chen, Y. Zhang, S. Chou, K. Lei, *Angew. Chem., Int. Ed.* **2024**, *63*, e202402946.
- [137] J. Li, Y. Hu, H. Xie, J. Peng, L. Fan, J. Zhou, B. Lu, *Angew. Chem., Int. Ed.* **2022**, *61*, e202208291.

Manuscript received: February 14, 2025

Revised manuscript received: March 18, 2025

Version of record online: March 20, 2025